https://doi.org/10.5194/acp-2021-118
Preprint. Discussion started: 24 February 2021

Atmospheric Chemistry and Physics Discussions

Evolution of OH reactivity in low-NO volatile organic compound photooxidation investigated by the fully explicit GECKO-A model

Zhe Peng[1], Julia Lee-Taylor[1,2], Harald Stark[1,3], John J. Orlando[2], Bernard Aumont[4] and Jose L. Jimenez[1]

[1] Department of Chemistry and Cooperative Institute for Research in Environmental Sciences, University of Colorado, Boulder, Colorado 80309, USA
[2] Atmospheric Chemistry Observation and Modeling Laboratory, National Center for Atmospheric Research, Boulder, Colorado 80307, USA
[3] Aerodyne Research Inc., Billerica, Massachusetts 01821, USA
[4] Laboratoire Inter-Universitaire des Systèmes Atmosphériques (LISA), UMR 7583, Université Paris-Est Créteil, Université de Paris, CNRS, Institut Pierre Simon Laplace, 94010 Créteil, France

Correspondence to: Zhe Peng (zhe.peng@colorado.edu) and Jose L. Jimenez (jose.jimenez@colorado.edu)

Abstract. OH reactivity (OHR) is an important control on the oxidative capacity in the atmosphere but remains poorly constrained. For an improved understanding of OHR, its evolution during oxidation of volatile organic compounds (VOCs) is a major aspect requiring better quantification. We use the fully explicit Generator of Explicit Chemistry and Kinetics of Organics in the Atmosphere (GECKO-A) model to study the OHR evolution in the low-NO photooxidation of several VOCs, including decane (an alkane), m-xylene (an aromatic), and isoprene (an alkene). Oxidation progressively produces more saturated and functionalized species. Total organic OHR (including precursor and products, OHR_{VOC}) first increases for decane (as functionalization increases OH rate coefficients), and m-xylene (as much more reactive oxygenated alkenes are formed). For isoprene, C=C bond consumption leads to a rapid drop in OHR_{VOC} before significant production of the first main saturated multifunctional product, i.e., isoprene epoxydiol. The saturated multifunctional species in the oxidation of different precursors have similar average OHR_{VOC} per C atom. The latter oxidation follows a similar course for different precursors, involving fragmentation of multifunctional species to eventual oxidation of C1 and C2 fragments to CO_2, leading to a similar evolution of OHR_{VOC} per C atom. An upper limit of the total OH consumption during complete oxidation to CO_2 is roughly 3 per C atom. We also explore the trends in radical recycling ratios. We show that differences in the evolution of OHR_{VOC} between the atmosphere and an environmental chamber, and between the atmosphere and an oxidation flow reactor (OFR) can be substantial, with the former being even larger, but these differences are often smaller than between precursors. The Teflon wall losses of oxygenated VOCs in chambers result in substantial deviations of OHR_{VOC} from atmospheric conditions, especially for the oxidation of larger precursors, where multifunctional species may suffer near-complete wall losses, resulting in significant underestimation of OHR_{VOC}. For OFR, the deviations of OHR_{VOC} evolution from the atmospheric case are mainly due to significant OHR contribution from RO_2 and lack of efficient organic photolysis. The former can be avoided by lowering the UV lamp setting in OFR, while the latter is shown to be very difficult to avoid. However, the former may significantly offset the slowdown in fragmentation of multifunctional species due to lack of efficient organic photolysis.

https://doi.org/10.5194/acp-2021-118
Preprint. Discussion started: 24 February 2021

Atmospheric Chemistry and Physics Discussions

1 Introduction

Photooxidation is a key process altering the concentrations of trace gases in the atmosphere (Levy II, 1971; Atkinson and Arey, 2003). It is also the main contributor to the formation of O_3 and secondary aerosols (Haagen-Smit, 1952; Chameides et al., 1988; Hallquist et al., 2009). Both products are major tropospheric pollutants (Nel, 2005; Cohen et al., 2017) and the latter have large climate impacts (Stocker et al., 2014).

Hydroxyl radical (OH) is the primary oxidizing agent in atmospheric photooxidation (Levy II, 1971). Its atmospheric fate is governed by the species that it reacts with, i.e., OH reactants. The first-order rate constant of OH consumption by an OH reactant is often called its OH reactivity (OHR), equal to the product of the reactant concentration and second-order rate constant with OH. Total OHR (OHR_{tot}), i.e., the sum of OHR across all OH reactants ($OHR_{tot} = \sum_i (k_i * c_i)$, where k_i and c_i are the second-order rate constant with OH and concentration of the ith OH reactant), is the real first-order loss rate constant of OH.

OHR has been measured for over 20 years (Kovacs and Brune, 2001) in various settings, e.g., urban areas (Lu et al., 2013; Whalley et al., 2016), forested areas (Nölscher et al., 2016; Zannoni et al., 2016), and environmental chambers (Nehr et al., 2014; Nölscher et al., 2014). Despite numerous measurements and remarkable technical developments (Yang et al., 2016; Fuchs et al., 2017), a sizable fraction of total OHR in most measurements has not been chemically speciated, leading to so-called "missing reactivity" (Williams and Brune, 2015; Yang et al., 2016). Multiple studies (Nölscher et al., 2016; Whalley et al., 2016; Sato et al., 2017) have attributed missing reactivity to the highly complex mixture of intermediates and products of volatile organic compound (VOC) oxidation, most of which are oxygenated VOCs (OVOCs). Primary VOCs themselves have been found to be the largest contributor of the speciated OHR in many studies (Yang et al., 2016). In order to well understand ambient OHR, the evolution of OHR (including that from OVOCs) during primary VOC photooxidation thus needs to be investigated.

Experimentally, this can be done in environmental chambers. However, only a few such experiments have been published (Nakashima et al., 2012; Nehr et al., 2014; Nölscher et al., 2014; Sato et al., 2017), all under high-NO conditions, where the key organic radical intermediate in VOC oxidation, i.e., organic peroxy radical (RO_2), mainly reacts with NO. To our knowledge, no experiment of this type at low NO, where RO_2 can substantially react with hydroperoxy radical (HO_2), has been published so far, probably due to the high difficulty in achieving low-NO conditions in chambers. Also, many OVOCs, which may account for missing reactivity, have sufficiently low volatility to significantly partition to chamber walls (Matsunaga and Ziemann, 2010; Krechmer et al., 2016), further complicating these experiments. The OVOC wall losses also often limit operation times of chamber experiments to a few hours, after which the wall losses are so large that meaningful interpretation of experimental results would be difficult. Therefore, the highest equivalent photochemical age that can be reached in chamber experiments is also typically hours and far shorter than would be needed to explore the OHR evolution in later stages of VOC oxidation.

Oxidation flow reactors (OFR) are an alternative to chambers with much smaller volume, shorter residence time (and thus smaller wall losses of trace gases), and stronger oxidative capacity (Kang et al., 2007; Brune, 2019; Peng and Jimenez, 2020). The most common version of OFR is equipped with low-

https://doi.org/10.5194/acp-2021-118
Preprint. Discussion started: 24 February 2021

Atmospheric Chemistry and Physics Discussions

pressure Hg lamps emitting UV at 185 and 254 nm, which photolyzes water vapor, O_2, and O_3, and generates a large amount of OH both directly and through subsequent radical reactions. High OH concentration in OFR often leads to equivalent photochemical age of days to weeks (Li et al., 2015; Peng et al., 2015). In principle, OFR can also be employed to explore OHR evolution in VOC oxidation. However, OHR from VOC (OHR_{VOC}, from both precursor and oxidation intermediates/products, in which we include CO as an "organic" product of VOC oxidation) can have strong impacts on oxidative capacity (particularly OH concentration) and hence radical chemistry in OFR at both low (Li et al., 2015; Peng et al., 2015) and high NO (Peng and Jimenez, 2017; Peng et al., 2018). Peng and Jimenez (2020) have called for highly chemically detailed modeling of gas-phase organic chemistry in OFR to assess the impacts of organic OH reactants on OH in a more quantitative manner.

In this study, we explore for the first time the OHR evolution in entire low-NO VOC photooxidation processes by modeling. Since chemical mechanism incompleteness causes other models to unsatisfactorily simulate measured OHR_{tot} (Williams and Brune, 2015), we use the fully chemically explicit model GECKO-A (Generator of Explicit Chemistry and Kinetics of Organics in the Atmosphere) (Aumont et al., 2005). We simulate the photooxidation of different types of VOCs in the atmosphere, in chamber, and in OFR, to find out general trends of OHR evolution in VOC oxidation and whether VOC oxidation chemistries in chamber and OFR are representative of that in the atmosphere in terms of OHR evolution.

2 Methods

Here we first discuss the VOC precursor types and conditions selected for the model cases in this study. Then we describe the GECKO-A model and present our additional mechanism, model, and software development required for this study.

2.1 Model cases

The photooxidation of an alkane (decane), an alkene (isoprene), and an aromatic (m-xylene) is investigated under a variety of conditions without any NO. In pristine regions such as open oceans, NO has typical concentrations on the order of 1 ppt (Wofsy et al., 2021) and hence contribute only a few percent to RO_2 loss (Peng et al., 2019). For simplicity, we choose not to maintain such a low NO level in the simulations, but to model zero-NO cases instead. The model cases are listed in Table 1: i) two cases under ambient conditions, one with constant sunlight at solar zenith angle of 45° and the other with diurnally-varying solar radiation and a noontime solar zenith angle of 0°; ii) four cases under typical chamber conditions, i.e., low (10 s^{-1}) / high (100 s^{-1}) precursor OHR with / without gas-particle-wall partitioning; and iii) five cases under OFR conditions, of which two conditions resulting in significant non-tropospheric organic photolysis (Peng et al., 2016) and one leading to remarkable deviations of RO_2 fate from that in the troposphere are not recommended in practice, but are still included for completeness since they are similar to conditions in some literature studies (Table 1). For the UV source in chamber cases, we adopt the spectrum of the blacklight and fluorescence light array in the University of Colorado Environmental Chamber Facility (CU Chamber; Krechmer et al., 2017). The parameterization for the reversible gas-wall partitioning is taken from Krechmer et al. (2016) with updates of Liu et al. (2019). The cases under ambient conditions, and chamber conditions with low / high precursor OHR are simulated for 10, and 6 / 30 d, respectively, to encompass an equivalent photochemical age of >10 d in

https://doi.org/10.5194/acp-2021-118
Preprint. Discussion started: 24 February 2021

Atmospheric Chemistry and Physics Discussions

each case (given a typical average ambient OH concentration of $1.5x10^6$ molecules cm^{-3} in the real atmosphere (Mao et al., 2009); see Fig. 1 for the correspondence between equivalent photochemical age and OH exposure (OH_{exp}, i.e., the integral of OH concentration over time)). The simulated OFR in the present work employs the light source parametrization obtained by Li et al. (2015) and Peng et al. (2015). UV at both 185 and 254 nm is used to generate OH, i.e., the "OFR185" mode of operation. The residence time in the OFR is always 3 min.

In addition, we simulate illustrative cases of methane oxidation, under ambient and OFR conditions (Table 1 and Section 3.1). Note that these two simulations are performed using the GECKO-A generated mechanism (see Section 2.2) in another chemical-kinetics solver, KinSim (Peng and Jimenez, 2019), to avoid possible numerical issues, as methane oxidation by OH is very slow (Atkinson and Arey, 2003) and very long runs are needed. To characterize trends of OHR evolution (see Section 3.5), the ambient cases with constant sunlight are simulated for two more alkanes, i.e., butane and heptane (Table 1). To explore the effects of UV sources in OFR (see Section 3.4), two simulations under a typical OFR condition with an additional broad-spectrum UV source (5 and 10000 times the chamber UV source in this study, respectively) are performed for isoprene (Table 1).

2.2 The GECKO-A model

GECKO-A (Aumont et al., 2005; Camredon et al., 2007; Valorso et al., 2011), is an explicit chemical model which uses known mechanisms and rates supplemented with experimentally-based structure-activity relationships to generate comprehensive atmospheric oxidation mechanisms for organic species. The mechanisms are implemented within a box model with a two-step solver (Verwer, 1994; Verwer et al., 1996). In mechanism generation, isomer lumping for mechanism reduction purposes is applied to certain products with branching ratios < 1% (here typically N-containing products, which are not relevant for our simulations). It has a negligible impact on the results.

The core isoprene scheme in GECKO-A is adopted from Master Chemical Mechanism v3.3.1 (Jenkin et al., 2015), while the meta-xylene oxidation mechanism follows MCM v3.2 (Jenkin et al, 2003, Bloss et al, 2005) until ring-breaking occurs, whereupon the GECKO-A mechanism generator implements the standard SAR protocols.

We tested the effect of solver integration timestep length on output precision. The output species concentrations in all simulations but for isoprene OFR (Table 1) converge well as integration timestep decreases (Fig. S1). In the isoprene OFR test cases, the output values oscillate over a small range (<~5%) for integration timesteps ≤ 0.01 s (Fig. S1). Since this numerical error is smaller than typical rate constant measurement uncertainties (from ~10% to a factor of 2–3; Burkholder et al., 2015), let alone the uncertainties related to the SARs used in GECKO-A, it is deemed acceptable for the relevant simulations in this study. The integration timestep for each simulation in the present work is reported in Table 1.

We allow mechanism generation to proceed through to CO_2 production in most cases in this study. The only exception is for extremely low-volatility species (saturation vapor pressure < 10^{-13} atm) which are considered to be completely and irreversibly partitioned to the particle phase. Particle- and wall-phase species are no longer considered in the OHR budget, since heterogeneous oxidation is much slower than gas-phase oxidation (e.g., George and Abbatt, 2010). Gas-particle-wall partitioning is activated only for the chamber cases where wall effects are considered. For the ambient cases and the chamber cases

https://doi.org/10.5194/acp-2021-118
Preprint. Discussion started: 24 February 2021

Atmospheric Chemistry and Physics Discussions

without gas-wall partitioning, gas-particle partitioning is also disabled to avoid artificial condensation of gases into the particle phase. In environments with very low NO (e.g., remote atmosphere), organic aerosol concentration is typically 0.2 μg m^{-3} (Hodzic et al., 2020) while most major intermediates/products have higher saturation concentrations (C*) and hence largely stay in the gas phase. C* is calculated using the parameterization of Nannoolal et al. (2008) (default option of GECKO-A). Although SIMPOL (Pankow and Asher, 2008) was recommended by Krechmer et al. (2016) to estimate C* for the chamber wall partitioning treatment using their parameterization, the C* estimates by the Nannoolal and SIMPOL parameterizations are close (generally within a factor of 2) for the species that can reversibly partition between the gas and wall phases (C* ~ 0.1–1000 μg m^{-3}) in this study. This difference is smaller than the uncertainties of the Krechmer et al. (2016) parameterization. Therefore, the use of the parameterization of Nannoolal et al. (2008) for C* estimation is acceptable.

Concerns have previously been expressed about non-conservation of carbon in GECKO-A (Mouchel-Vallon et al., 2020). This has proven in the current simulations to be almost entirely due to lack of accounting for product CO_2 in some handwritten reactions. We edited the handwritten isoprene and m-xylene schemes (see above and Section 2.2.3) for carbon balance, which reduced simulation-end carbon losses in the m-xylene and isoprene ambient cases with constant UV from 4% and 9%, respectively, to negligible levels (<0.4%; Fig. S2).

For the current study, we have made several updates to GECKO-A, i.e., i) inclusion of key OFR-specific radical reactions, ii) extension of the UV range considered to cover 185 and 254 nm, and iii) updates to the low-NO m-xylene oxidation mechanism, so that GECKO-A is able to simulate OFR chemistry and the entire process of low-NO m-xylene photooxidation (until CO/CO_2). We will describe these three updates below.

2.2.1 Key radical reactions in oxidation flow reactor

We have added several reactions that are unimportant in the troposphere, but that are required to fully represent the radical chemistry within the OFR (Li et al., 2015). The most important inorganic reactions are $H_2O + h\nu$ (185 nm) → H + OH, $O_2 + h\nu$ (185 nm) → $2O(^3P)$, and $O_3 + h\nu$ (254 nm) → $O(^1D) + O_2$. These three reactions, together with $O(^3P) + O_2 + M \rightarrow O_3 + M$ and $O(^1D) + H_2O \rightarrow 2OH$, which are already in the GECKO-A inorganic radical chemistry scheme, are responsible for the OH generation in OFR. The OFR radical chemistry has previously been modeled in detail using KinSim (Peng and Jimenez, 2019), which was validated against experimental observations (Li et al., 2015; Peng et al., 2015). A comparison between KinSim and GECKO-A for a range of OFR conditions shows typical agreement between the two models within 2% for key outputs.

Due to high OH in OFR, reaction of RO_2 with OH is also included in mechanism generation, with an assumed rate constant of $1x10^{-10}$ cm^3 $molecule^{-1}$ s^{-1} (Peng et al., 2019). The products of this type of reaction are assumed to be RO (alkoxy radical) + HO_2 for alkyl RO_2 and R (alkyl radical) + CO_2 + HO_2 for acyl RO_2. Although these reactions for certain RO_2 may have reaction intermediates, the reactions of the intermediates are believed to be very fast in OFR (Peng and Jimenez, 2020) and hence only the probable final products (no intermediates) of these reactions are included in mechanism generation. The reaction of RO_2 with OH is not included in the mechanisms for the ambient and chamber simulations due to low contribution of this pathway to the RO_2 fate in those cases.

https://doi.org/10.5194/acp-2021-118
Preprint. Discussion started: 24 February 2021

Atmospheric Chemistry and Physics Discussions

2.2.2 Organic photolysis at 185 and 254 nm

Organic photolysis is assessed in GECKO-A via a lookup table of j-values for reference chromophores pre-calculated at different solar zenith angles with the TUV 1-D radiative transfer model (Madronich and Flocke, 1999). The reference cross-sections used in the model generally do not cover the UV wavelengths at which OFR operates (with narrow peaks at 185 nm and 254 nm) since they are not tropospherically relevant. Thus it was necessary to extend to 185 nm the relevant reference absorption cross-sections. We have done this using literature values via the Mainz UV-Vis spectral atlas (Keller-Rudek et al., 2020) or by extrapolating the available cross-section data, using other similar chromophores as references. Details of all cross-section extensions are given in Table S1. Where quantum yield information was not available, we assume values of unity since photons at 185 and 254 nm are usually sufficiently energetic to make photolysis occur (Ausloos and Lias, 1971). In case of multiple product channels for a photolyzed molecule, the branching ratios of those channels at 185 and 254 nm are estimated through extrapolation of branching ratio data from available ranges followed by a renormalization. Finally, we apply the OFR UV spectrum within TUV to calculate OFR-relevant j-value lookup tables.

2.2.3 Mechanism of low-NO m-xylene oxidation

The meta-xylene oxidation mechanism in GECKO-A follows MCM v3.2 until all aromatic, epoxy, or bridged-peroxy rings are broken (See Scheme S1). Since the MCM was designed for typical urban environments with abundant NO_x, it omits some reaction pathways for other oxidants, assuming them to be of negligible importance. The relevant photolysis loss pathways are slow under ambient conditions and inactive in the OFR case. This leads to persistence and accumulation of certain hydroperoxides and their interconverting peroxy radicals under low-NO conditions. We added two low-NO oxidation reactions to the xylenol branch of the meta-xylene oxidation scheme, Scheme S1. In the 51% branch, we allow the unsaturated bicyclic peroxide "MXYLOOH" to react with, sequentially, OH (estimating $k_{OH} \sim 3e^{-11}$ cm^3 molecule^{-1} s^{-1}) and HO_2 (estimating $k_{RO2+HO2} \sim 1e^{-11}$ cm^3 molecule^{-1} s^{-1}), to produce a saturated bicyclic peroxide (denoted "TT8001" in Scheme S1). In the 42% branch, we add a competing O_3 reaction with the alkoxy radical "MXCATEC1O", producing an unsaturated carbonyl alkoxy radical "1T8000" which eliminates CH3 to form the unsaturated cyclic hydroxy dicarbonyl "TU7000". Both products are then further oxidised via the standard GECKO SARs.

2.3 GECKO Loader and Plotter

To allow GECKO-A outputs, which are usually highly complex and voluminous, to be explored and visualized in detail on standard (non-UNIX) personal computers, we have developed the GECKO Loader and Plotter based in the data-analyzing and graphic-making package Igor Pro 8.0 (WaveMetrics, Lake Oswego, Oregon, USA). This tool assists on the rapid and detailed analysis of model-chamber/OFR comparison studies.

Specifically, the GECKO Loader and Plotter facilitates: i) filtering the (sometimes extremely large and finely-resolved) model results time series to examine specific characteristics, ii) identifying the most abundant and/or influential species in each phase (gas, particle, and wall), iii) selecting species by specific chemical identity (molecular formula, specific formula, and/or functional group identity), iv) plotting time series of individual species and their formation/destruction rates, v) assessing and

https://doi.org/10.5194/acp-2021-118
Preprint. Discussion started: 24 February 2021

Atmospheric Chemistry and Physics Discussions

displaying aggregated properties (volatility distribution, mass spectrum, Henry's law constant distribution) of the product mixture and subsets thereof, and vi) calculating bulk characteristics of the simulation (OH_{exp}, OHR_{VOC}, light intensity, elemental ratios etc.) and relating species abundances to them.

3 Results and discussions

In this section, we will show the evolution of OHR_{VOC} in the photooxidation of different precursors under various conditions. To aid the presentation of this evolution for larger precursors, whose oxidation is more complex, the oxidation of the simplest VOC, i.e., methane, will be first discussed. After presenting the results of individual precursors, we will compare the results between conditions and between precursors to illustrate the general trends. Along with the OHR evolution, OH recycling ratio (β_1, defined as number of OH molecules generated from organic reactions per OH consumed by organics) and HO_x (= OH + HO_2) recycling ratio (β_2, defined as number of OH and HO_2 molecules generated from organic reactions per OH consumed by organics) will also be discussed, as they are important parameters that may considerably affect the budget of atmospheric oxidizing agents (Stone et al., 2012) and the HO_2-to-OH ratio and RO_2 chemistry in OFR (Peng et al., 2015, 2019).

3.1 Methane

To explain one of the main features in the OHR evolution in VOC photooxidation, i.e., OHR_{VOC} peaking at a certain OH_{exp}, the oxidation of CH_4 is employed as an example because of its simpler mechanism (Scheme S2). The results of this oxidation under the ambient condition show that OHR_{VOC} peaks at an OH_{exp} of about $1x10^{13}$ molecules cm^{-3} s (Fig. S3). As the OHR of the precursor always decreases during its oxidation, the appearance of such a peak of OHR_{VOC} before all VOCs are finally oxidized to CO_2 indicates that the OHR increase from intermediates and products is faster than the OHR decrease of the precursor. This is obviously the case for CH_4 oxidation, as there is no significant CH_4 loss before $OH_{exp} \sim 10^{13}$ molecules cm^{-3} s by its very slow reaction with OH (rate constant on the order of 10^{-15} cm^3 $molecule^{-1}$ s^{-1}; Atkinson and Arey, 2003) and all the non-CO_2 intermediates/products of the oxidation (CH_3OOH, CH_3OH, HCHO, and CO) are orders of magnitude more reactive toward OH than is CH_4 (Atkinson and Arey, 2003). This large difference in precursor and intermediate/product oxidation timescales allows the oxidations of intermediates/products (including CO, whose reaction rate constant with OH is ~$2x10^{-13}$ cm^3 $molecule^{-1}$ s^{-1}; Burkholder et al., 2015) to establish a steady state, whereby the OHR of the intermediates/products is proportional to the concentration/OHR of CH_4. After $OH_{exp} \sim 10^{13}$ molecules cm^{-3} s, CH_4 concentration decay, and consequently that of all intermediates/products, become significant, giving the OHR_{VOC} peak around $1x10^{13}$ molecules cm^{-3} s.

We also performed a simulation under a typical OFR condition. The OHR_{VOC} peak also appears around $1x10^{13}$ molecules cm^{-3} s in this case for the same reasons discussed above, but its height is almost twice that of the ambient case (Fig. S3). The OHR of CO in both cases is similar, while that of CH_3OH is higher in the ambient case but those of CH_3OOH and HCHO are significantly higher in the OFR case. This is because the relative importance of the various reactions involved in CH_4 oxidation (Scheme S2) depends on the conditions in each reactor.

In the OFR case, OH and HO_2 concentrations are ~4 and ~3 orders of magnitude higher than typical ambient values, respectively (Peng et al., 2015). The reactions of two intermediates, CH_3OOH

https://doi.org/10.5194/acp-2021-118
Preprint. Discussion started: 24 February 2021

Atmospheric Chemistry and Physics Discussions

and HCHO, with OH and the reaction of the only major RO_2 involved, CH_3OO, with HO_2 are much faster than their photolysis or the self-reaction of CH_3OO (Scheme S2). Neglecting organic photolysis and CH_3OO self-reaction (and thus CH_3OH as a product of the latter), the mechanism of CH_4 oxidation can be simplified to an OH-driven chain ($CH_4 \rightarrow CH_3OOH \rightarrow HCHO \rightarrow CO \rightarrow CO_2$) with a fast steady-state branch on CH_3OOH ($CH_3OOH \leftrightarrow CH_3OO$). For a simple chain, as we show in Appendix A, the OHR of precursor and that of each intermediate are equal. At the OHR_{VOC} peak, the OHR of HCHO and CO are very close to that of CH_4, while that of CH_3OOH is larger, because the branch reaction $CH_3OOH + OH \rightarrow CH_3OO + H_2O$ also contributes to OHR, but does not affect the chain (and hence the OHR of the downstream species). With such an idealized chain mechanism, the OHR_{VOC} peak height equals the precursor OHR multiplied by the number of steps needed to produce CO_2.

In contrast, the OHR_{VOC} peak height (and its composition) in the ambient case cannot be explained by the simple chain. Both HCHO photolysis and CH_3OO self-reaction play a major role in the oxidation in this case, and are significantly faster than the reactions in the simple chain (HCHO + OH and $CH_3OO + HO_2$). In terms of the relationship of these two reactions with the chain, HCHO photolysis bypasses HCHO + OH in converting HCHO to CO, while CH_3OO self-reaction bypasses CH_3OOH, in effect short-circuiting the involvement of OH in the oxidation and hence lowering OHR_{VOC} (Appendix A). Since the only reaction of CO is CO + OH, its OHR at the OHR_{VOC} peak is essentially unaltered.

3.2 Decane

3.2.1 Ambient and OFR cases

The evolution of OHR_{VOC} during the oxidation of another alkane, decane, under ambient and OFR conditions exhibit a smaller difference and smaller peak enhancements than those in the methane cases (Fig. 1), although the chain lengths of the decane oxidation to CO_2 should be much longer than that of methane. The ambient cases with constant and diurnal solar radiation have almost the same OHR_{VOC} evolution as a function of OH_{exp} (Figs. 1 and 2). Contrary to the methane cases, OHR_{VOC} in all five decane simulations for OFR conditions is lower than that for ambient conditions.

These differences from the methane cases arise because a key assumption of the simple reaction chain model, i.e., slow precursor decay allowing intermediates/products to build up and reach a steady state, no longer holds in decane oxidation. The main first-generation products, i.e., secondary decyl hydroperoxides, react with OH only < x3 more rapidly than does decane, as the significant activation effect of the –OOH group only applies to the α-H, and all other H atoms in this long chain alkyl can, though less reactive, be abstracted by OH (Kwok and Atkinson, 1995; Aumont et al., 2005). When decyl hydroperoxides are present in significant amounts ($OH_{exp} \sim 5x10^{10}$ molecules cm^{-3} s), decane loss is also significant (Fig. 3). Also, oxidation of monohydroperoxides to ketones, their most likely fate (due to the activated α-H), lowers OHR_{VOC}, as the oxidation removes the most activated H (Kwok and Atkinson, 1995). The multifunctional products of further oxidation in the mid OH_{exp} range (before $\sim 2x10^{11}$ molecules cm^{-3} s), mainly have -OOH and -CO- (Fig. 4), which do not further increase OHR substantially with respect to monohydroperoxides, for similar reasons as the comparison of monohydroperoxides with decane. After the OHR_{VOC} peak, the precursor is largely consumed and -CH(OOH)- groups become increasingly oxidized to -CO- in both monohydroperoxides and multifunctional hydroperoxides (Figs. 3 and 4), which rapidly decreases OHR_{VOC}. Since the decane oxidation chain does not reach a steady state,

https://doi.org/10.5194/acp-2021-118
Preprint. Discussion started: 24 February 2021


Atmospheric Chemistry and Physics Discussions

it results in only limited OHR_{VOC} enhancement at peak.

The differences between the ambient and OFR cases for decane oxidation are for different reasons than in the case of CH_4. In the absence of steady state for the nodes (stable species) in the decane oxidation chains (nodes far downstream insufficiently populated), organic photolysis and RO_2 self- and cross-reactions only help move OHR contributors to downstream nodes, but do not significantly change their total concentrations. This is shown by the relatively small differences in the composition of stable OHR contributors between the ambient and OFR cases (Fig. 3). The remarkable difference between these cases is the contribution of RO_2 to OHR, which is as high as ~3 s^{-1} in the OFR case shown in Fig. 3, while estimated to be only up to ~0.1 s^{-1} in the ambient case, given the RO_2 concentration in the simulation.

It is known that RO_2 + OH can be a significant RO_2 loss pathway in OFR, especially when OH and HO_2 production is relatively strong (higher relative humidity (RH) and UV). We have previously advised to avoid such conditions in low-NO chemistry based on simplified modeling, because of its high-NO-like organic product (Peng et al., 2019). Here our chemically explicit modeling results show that the limitation for OFR chemistry caused by RO_2 + OH may not be as serious as suggested by Peng et al. (2019), at least in terms of OHR_{VOC} and, to some extent, of organic composition (Fig. 3). The condition of the OFR case shown in Fig. 3 (30% RH, medium UV, and 10 s^{-1} initial OHR) is a compromise between the goals of reaching an equivalent photochemical age of ~10 d, avoiding significant non-tropospheric organic photolysis, and keeping a more atmospherically relevant RO_2 chemistry (Peng et al., 2016; Peng et al., 2019; Peng and Jimenez, 2020). In this case, the fractional contribution of RO_2 + OH to RO_2 fate is still sizable (>30%). However, the evolution of the composition of monofunctional species in this OFR case before the OHR_{VOC} peak equivalent age is similar to that in the ambient case (Fig. 3), as hydroperoxide production through RO_2 + HO_2 is still the main loss pathway of the first-generation RO_2 and RO produced from RO_2 + OH can also form ketones, i.e., the main second-generation products. The other main fate of RO, i.e., isomerization, leads to slightly faster production of multifunctional species, since the product of the recombination of the immediate product of this isomerization, i.e., an alkyl radical, with O_2 is already a bifunctional RO_2. This isomerization also creates a hydroxyl group on the C backbone, resulting in a relatively high share of hydroxyl in the functional groups of the multifunctional species (Fig. 4).

Before the OHR_{VOC} peak, as OH_{exp} increases, carbonyls accumulate. They are prone to Norrish-type photochemistry (Turro et al., 2009) which plays a major role in the OHR evolution after the OHR_{VOC} peak in the ambient cases by breaking C10 species into smaller molecules (Fig. 3). Alkenes, which can only be produced via Norrish Type II reaction in this case (Turro et al., 2009), are non-negligible OHR contributors around $3x10^{11}$ molecules cm^{-3} s. A set of oxygenated C1 and C2 species are also largely produced through organic photolysis followed by reactions with (O_2 and) HO_2. Organic photolysis, along with OH reaction pathways, can also produce RO_2. Self- and cross-reactions of acylperoxy radicals, which are formed in significant amounts in this OH_{exp} range, can rapidly generate alkoxy radicals (Orlando and Tyndall, 2012), which may decompose subsequently (Ziemann and Atkinson, 2012). At ~$1x10^{12}$ molecules cm^{-3} s, the small species produced account for about half of OHR_{VOC} in the ambient cases (Fig. 3). In the OFR cases, organic photolysis is usually much weaker than in the atmosphere (Peng

https://doi.org/10.5194/acp-2021-118
Preprint. Discussion started: 24 February 2021

Atmospheric Chemistry and Physics Discussions

et al., 2016; Peng and Jimenez, 2020), as the negligible OHR of alkenes in the OFR case in Fig. 3 also indicates. However, fragmentation of multifunctional species does not appear to be significantly weaker in the OFR case than in the ambient case shown in Fig. 3. This is largely due to fast RO_2 + OH. The reactions of acylperoxys with OH lead to direct fragmentation (Orlando and Tyndall, 2012). Highly functionalized RO can also form from the reactions of multifunctional RO_2 with OH, and then often rapidly decompose. RO_2 + OH also results in a major difference of the OFR case from the ambient case at high equivalent ages (Fig. 3), i.e., lower (higher) OHR contribution from CH_3OOH (HCHO) in OFR than in the atmosphere. Most CH_3OO reacts with OH to produce CH_3O then HCHO in the OFR case, leaving a minor fraction of CH_3OO reacting with HO_2 to form CH_3OOH.

3.2.2 Chamber cases

Two types of chamber simulations, with and without wall partitioning, are considered in this study. The latter have almost the same results as the ambient cases in terms of the evolution of OHR_{VOC} and its composition as a function of OH_{exp} (Fig. 1). Despite different spectra, sunlight and chamber lights cover the same wavelength range and usually generate oxidizing agent radicals (e.g., OH and HO_2) in similar amounts. Therefore, all key parameters are very similar between the ambient case with constant solar radiation and the chamber case (with 10 s^{-1} initial OHR) and without gas-wall partitioning. This explains the high similarities between the results of the ambient cases and the chamber cases without wall partitioning. Unfortunately, the lack of wall partitioning is not realistic.

The chamber cases with gas-wall partitioning, which are realistic, show very large deviations from the ambient cases (Figs. 1 and 3). These deviations are remarkably larger than those of the OFR cases, and are obviously due to wall partitioning of OVOCs. The wall removes more than half of the OHR of decane oxidation intermediates/products (Figs. 1 and 2) and hence also removes the OHR_{VOC} peak in the relevant chamber cases (Fig. 1). In detail, about half of decyl hydroperoxides partition to the wall in the chamber case shown in Fig. 3, as decyl is a relatively large alkyl and leads to hydroperoxides of sufficiently low volatility to promote wall partitioning. The C10 ketones, usually of higher volatility than the corresponding hydroperoxides, do not show significant wall partitioning (Fig. 3), while the multifunctional C10 species, of even lower volatility than the corresponding hydroperoxides, are almost completely partitioned to the wall. The multifunctional species that survive the wall partitioning at high OH_{exp} (~$1x10^{12}$ molecules cm^{-3} s) are formed via C10 fragmentation and are thus of higher volatility (Fig. 3). The heavy wall partitioning of multifunctional species also significantly slows down their oxidative evolution in both the wall phase and the gas phase relative to the ambient cases (Fig. 4).

As OH_{exp} increases and large multifunctional species are formed in increasing amounts from oxidation, their near-complete partitioning to the wall decreases the OHR of decane oxidation intermediates/products by a factor up to 8 around $1x10^{12}$ molecules cm^{-3} s compared to the chamber cases without gas-wall partitioning (Fig. 2). At higher OH_{exp} (long oxidation times) gas-phase concentrations of partitioning species decline, allowing reverse partitioning back from the wall which then serves as a source rather than a sink. As a result, the ratio of the OHR of oxidation intermediates/products in the chamber case with wall partitioning to that without wall partitioning decreases (Fig. 2).

3.2.3 OH and HO_x recycling ratios

As discussed above, we also compute OH (β_1) and HO_x (β_2) recycling ratios in decane oxidation.

https://doi.org/10.5194/acp-2021-118
Preprint. Discussion started: 24 February 2021

Atmospheric Chemistry and Physics Discussions

Note that these quantities also include OH and HO_2 generated as a result of organic photolysis. The differences in these recycling ratios between the simulated cases are relatively small. β_1 is close to 0 at OH_{exp} < ~$1x10^{10}$ molecules cm^{-3} s (Fig. 1), as the initial reaction of decane with OH only produces an RO_2 and subsequently C10 hydroperoxides, and no HO_x. Then β_1 undergoes a fast increase between ~$1x10^{10}$ and $1x10^{11}$ molecules cm^{-3} s (Fig. 1), as the further oxidation of C10 hydroperoxides to ketones fully recycles OH (R_1-CH(OOH)-R_2 + OH → R_1-CO-R_2 + H_2O + OH) in the ambient and chamber cases. Nevertheless, β_1 only increases up to ~0.4 at this stage in the ambient and chamber cases, as oxidation of C10 hydroperoxides to dihydroperoxy species and precursor oxidation also account for a substantial fraction of OH loss but do not recycle it. In the OFR cases, β_1 only increases up to ~0.2–0.3 at this stage, since RO_2 + OH starts to be active but does not recycle OH. Then, β_1 roughly plateaus up to ~$1x10^{12}$ molecules cm^{-3} s, as the overall effect of the decrease in hydroperoxy concentration, reducing OH recycling, and the increase in the concentration of acylperoxy, enhancing OH recycling through its reaction with HO_2 (Orlando and Tyndall, 2012), is relatively small. Finally, β_1 gradually decreases to 0 (Fig. 1), as all OVOCs degrade to highly oxidized C1 species, i.e., HCHO, HCOOH, CO, which only have HO_2 recycling but no OH recycling, and the unreactive CO_2.

The HO_x recycling ratio (β_2) in decane oxidation is similar to β_1 before ~$1x10^{11}$ molecules cm^{-3} s for the ambient and chamber cases, as only OH (but not HO_2) is recycled at this stage. β_2 is a little higher in the OFR cases than in the other cases at this stage because of the HO_2 recycling by RO_2 + OH. However, at higher OH_{exp}, β_2 continues to increase with OH_{exp} to a final value of 1 (Fig. 1). This difference between β_1 and β_2 is by definition due to HO_2 recycling. Its significance rises in parallel with that of organic photolysis, which can often produce HCO radicals and acylperoxy radicals. The former extremely rapidly undergoes HCO + O_2 → CO + HO_2; the latter can rapidly convert peroxy radicals to alkoxy radicals (Orlando and Tyndall, 2012), which may then react with O_2 to generate HO_2 (Ziemann and Atkinson, 2012). At very high OH_{exp} (10^{12} – 10^{13} molecules cm^{-3} s), reactive highly oxidized small VOCs are the dominant OHR contributors and many of them recycle HO_2 during their oxidation by OH (Fig. 3). Finally, once CO becomes the only remaining OHR contributor, β_2 is 1.

3.3 m-Xylene

Most features in m-xylene oxidation can be explained based on similar discussions as for decane oxidation in Section 3.2. OHR_{VOC} also has a maximum during the oxidation (Figs. 1 and S4), as most of the direct products of m-xylene oxidation by OH, i.e., the unsaturated carbonyl (MXYEPOXMUC in MCM v 3.2 notation, see Scheme S1), the unsaturated endo-cyclic peroxide (MXYBIPERO2), and xylenols, are more reactive toward OH than m-xylene. The OHR of these initial products is enhanced much more during the oxidation of m-xylene than of decane, owing to the creation of C=C bonds in many post-aromatic (ring-opening) products, hence the OHR_{VOC} peak enhancement in m-xylene oxidation is larger than in decane oxidation. Because the reaction rate constant of m-xylene with OH slightly exceeds that of decane, the OHR_{VOC} peak in m-xylene oxidation occurs at slightly lower OH_{exp} than in decane oxidation (Fig. 1). In the OFR case under the same condition as the decane case shown in Fig. 3, the evolution of OHR of the stable organic species is again similar to that in the ambient case. And OHR_{VOC} is higher in the OFR case again mainly due to OHR from RO_2 (Fig. 1 and S4). Several main first- and second-generation products are already highly functionalized through fast O_2 addition

https://doi.org/10.5194/acp-2021-118
Preprint. Discussion started: 24 February 2021

Atmospheric Chemistry and Physics Discussions

(Scheme S1) and they are also often unsaturated and prone to further functionalization. Therefore, the degree of functionalization in saturated aliphatic multifunctional species is much higher in m-xylene than in decane oxidation (Fig. 4). Also, as several aromatic-scheme-specific reaction types occur in the early stages of m-xylene oxidation, e.g., endo O_2 addition (creating -OO- etc.) and ring-opening (creating -CO-, -CHO etc.), multifunctional species functionality is more diverse than in decane oxidation (Fig. 4). Photolysis again plays a role in species fragmentation and the production of highly oxidized C1 and C2 species after the OHR_{VOC} peak (Fig. S4).

Wall partitioning also substantially reduces the OHR_{VOC} in the relevant chamber cases of m-xylene oxidation (Figs. 1, 2 and S4). The precursor (m-xylene) is a C8 species and even many first-generation products of its oxidation are highly oxygenated (Scheme S1) lower-volatility species. The relative reduction of OHR of the intermediates/products also increases with OH_{exp} up to ~$1x10^{12}$ molecules cm^{-3} s, as volatile species are oxidized and become more prone to wall partitioning (Fig. 2). At higher OH_{exp}, the wall again serves as an OVOC source (Fig. 2).

The evolution of β_1 and β_2 in m-xylene oxidation is somewhat different than in decane oxidation (Fig. 1). In the ambient cases, they are non-negligible even at OH_{exp}.as low as $1x10^9$ molecules cm^{-3} s (~0.05 and ~0.45, respectively). OH is mainly recycled from one of endo-cyclic peroxide routes (m-xylene + OH + $2O_2$ → MXYBIPERO2; MXYBIPERO2 + HO_2 → MXYBPEROOH + O_2; MXYBPEROOH + OH → MXYOBPEROH + H_2O + OH (Scheme S1)), which involve various functional groups and open the possibility of radical recycling. The third step of this route is very fast (with a rate constant on the order of 10^{-10} cm^3 $molecule^{-1}$ s^{-1}). Once the second step takes place, the third step contributes to OH recycling. However, in the OFR cases with strong water vapor photolysis (not in the other OFR cases) and the chamber cases with gas-wall partitioning, the third step does not play a significant role and β_1 is ~0 at very low OH_{exp} (Fig. 1). In the former cases, this is due to the relatively slow second step (RO_2 + HO_2), while in the latter cases, the highly oxygenated compounds partition to the wall even more rapidly (in hundreds of s; Krechmer et al., 2016) than their reactions with HO_x. Strong HO_2 recycling occurs in all simulated cases from the beginning of the oxidation (Fig. 1), since two of the three major channels of m-xylene + OH (i.e., those forming MXYEPOXMUC and xylenol, respectively) produce HO_2 as well.

As more multifunctional species are formed (particularly through ring-opening) near the OH_{exp} of the peak OHR_{VOC}, HO_x recycling is also active, with β_1 increasing and β_2 remaining high (Fig. 1). There are a few peaks in β_1 and β_2 for certain chamber cases. The peak in β_2 for the chamber case with high initial OHR (100 s^{-1}) and no walls results from RO_2 cross-reactions, many of which produce alkoxy radicals that subsequently yield carbonyls and HO_2 through reactions with O_2 (Orlando and Tyndall, 2012). RO_2 cross-reactions are significant in that OH_{exp} range also because i) high precursor concentration translates into higher RO_2 concentration and ii) acylperoxy radicals, whose reactions with other RO_2 are fast (Orlando and Tyndall, 2012), are rapidly formed from the oxidation of -CHO groups in the ring-opening products (Scheme S1). The peaks in the chamber cases with wall partitioning are caused by a small number of species (in particular methylglyoxal) sufficiently volatile to stay in the gas phase and thus have disproportionate influence on β_1 and β_2. Methylglyoxal photolysis and the reaction of HO_2 with $CH_3COCO(OO)$, i.e., the acylperoxy formed through methylglyoxal + OH, are largely

https://doi.org/10.5194/acp-2021-118
Preprint. Discussion started: 24 February 2021

Atmospheric Chemistry and Physics Discussions

responsible for the HO_2 and OH recycling at the OH_{exp} of the peaks. At higher OH_{exp}, calculated β_1 and β_2 become less reliable, since remaining apparent OHR contributors may in fact be persistent artifacts of the incompleteness of the (hand-written) m-xylene oxidation mechanism which may substantially bias β_1 and β_2 when the concentrations of remaining OHR contributors should be generally low. Therefore, we do not try to interpret the features in β_1 and β_2 at high OH_{exp} for m-xylene oxidation.

3.4 Isoprene

The most salient difference of the OHR_{VOC} evolution in the photooxidation of isoprene from that of the other precursors in this study is the lack of OHR_{VOC} peak in the isoprene cases (Figs. 1 and S5). The decrease in OHR_{VOC} all along this photooxidation is expected since the reaction of isoprene with OH is very fast (at $1x10^{-10}$ cm^3 $molecule^{-1}$ s^{-1}; Atkinson and Arey, 2003) and all intermediates/products of this photooxidation react with OH more slowly than isoprene. The OHR_{VOC} of the intermediates/products peaks slightly after an OH_{exp} of $1x10^{10}$ molecules cm^{-3} s (Fig. 1). At this OH_{exp}, the main type of the first-generation products, oxygenated unsaturated species (e.g., isoprene-derived unsaturated hydroxyl hydroperoxides (ISOPOOH)), are largely produced from isoprene + OH and their loss rates (with rate constant with OH slightly lower than that of isoprene) reach the maxima (Fig. S5). Further oxidation leads to the loss of all C=C bonds in the isoprene C backbone and thus a substantial drop of the OHR of the molecule.

Before OH_{exp}~$5x10^{10}$ molecules cm^{-3} s in isoprene photooxidation, the main deviations from the ambient cases shown by the chamber cases with wall partitioning are again caused by wall partitioning of multifunctional species, but their relative magnitudes are different than in the photooxidations of decane and m-xylene, with the impacts of wall partitioning being smaller (Fig. S5). Oxygenated species derived from isoprene, a C5 species, should be generally more volatile and less prone to wall partitioning than those derived from decane and m-xylene. On the other hand, isoprene reacts with OH much more rapidly than do decane or m-xylene, creating a larger deviation from the steady state for RO_2 directly derived from isoprene and a more remarkable decrease in the OHR of the first-generation products (Fig. S5). In the OFR case shown in Fig. S5, RO_2 contributes negligibly to OHR_{VOC}, since many first-generation isoprene-derived RO_2 have other very fast loss pathways and the very fast decay of isoprene cannot sustain RO_2 production at OH_{exp}>~$1x10^{10}$ molecules cm^{-3} s.

After OH_{exp}~$5x10^{10}$ molecules cm^{-3} s, the deviation caused by chamber wall partitioning becomes more significant as highly oxidized and lower-volatility multifunctional species (Fig. 4) are formed in significant amounts (Figs. 2 and S5). At very high OH_{exp}, the wall again acts as a source of OVOCs in isoprene oxidation, as in those of the other precursors (Fig. 2). The deviations of OFR cases from the ambient cases are mainly caused by RO_2 + OH and lack of organic photolysis. These two effects lead to too much HCHO produced and inefficient production of other C1 and C2 species (Fig. S5).

To test whether one of the issues, i.e., lack of organic photolysis in OFR, can be mitigated by adding tropospherically-relevant UV sources, we perform two additional simulations. Adding the emissions corresponding to high Hg lamp setting with five times the UV of the CU Chamber (a rough upper limit for experimental implementation) has negligible effect (Fig. S6). To reach a ratio between tropospherically-relevant UV (UVA+UVB) intensity and OH concentration similar to that in the ambient case with constant sunlight requires addition of a chamber light ~10000 times stronger than the CU

https://doi.org/10.5194/acp-2021-118
Preprint. Discussion started: 24 February 2021

Atmospheric Chemistry and Physics Discussions

Chamber light. Such a strong UV source is obviously not realistic, and, while it does increase both early organic photolysis and the relative contribution of C1 and C2 photoproducts to OHR_{VOC} around $2x10^{11}$ molecules cm^{-3} s (Fig. S6), it increases the deviation of this OFR case from the ambient cases at very high OH_{exp}, where oxidation of C1 and C2 species to CO proceeds much more rapidly than in the atmosphere.

Product functionality in isoprene oxidation is more diverse than in decane oxidation (Fig. 4). This is due to both the propensity of the isoprene C=C bonds to addition of various groups, and the active isomerization of isoprene oxidation intermediates (Wennberg et al., 2018). Notably, epoxy groups in species such as isoprene-derived epoxydiol (IEPOX) account for a large fraction of saturated product functionality (Fig. 4), particularly at OH_{exp} on the order of 10^{10} molecules cm^{-3} s. In the gas phase of the chamber cases with wall partitioning, the overwhelming majority of saturated multifunctional organic molecules are IEPOX up to $1x10^{11}$ molecules cm^{-3} s (Fig. 4), as more highly-oxidized species mostly partition to the wall.

IEPOX formation from isoprene-derived hydroperoxide (ISOPOOH) oxidation by OH (ISOPOOH + OH → IEPOX + OH) leads to the peak of OH recycling around $3x10^{10}$ molecules cm^{-3} s (Fig. 1). OH recycling is active even at very low OH_{exp} ($1x10^{9}$ molecules cm^{-3} s) because a significant amount of ISOPOOH forms early and can recycle OH through its oxidation, except in the OFR cases with strong water vapor photolysis, where ISOPOOH cannot be efficiently formed from first-generation RO_2. HO_2 recycling is also active in the entire course of the photooxidation (Fig. 1), because of a number of isomerization and photolysis pathways that form alkoxy radicals and highly oxidized C1 species such as HCOOH, HCHO, and CO at very high OH_{exp} (Fig. S5).

3.5 Trends in OHR per C atom

To explore some general trends of OHR evolution in VOC photooxidation, simulations are performed for the ambient cases with constant UV for two additional alkanes between methane and decane, i.e., butane and heptane. The results of these simulations are compared to the existing analogous cases in Fig. 5. For all cases, the OHR_{VOC} peak height decreases and the OH_{exp} of the OHR_{VOC} peak shifts towards lower OH_{exp}, as the C number of the precursor alkane increases. This can be explained by the fact that the OH rate constants of these alkanes increase with C number, and suggests a possible general trend between OHR peak location and C number.

To explore these trends further, we calculate the OHR per unit starting concentration of C atom (in the precursor) in all ambient cases with constant UV in this study (Fig. 5b). In this study, CO_2 is not included initially but produced during the oxidation. Therefore, C atoms in the produced CO_2 are taken into account in the calculation of OHR per C atom. For real atmospheric cases, initial CO_2 is present but should not be considered in this calculation. Note that OHR per C atom has a unit of cm^3 $atom^{-1}$ s^{-1} and represents the average contribution to the rate constant with OH of all considered C atoms. Despite large differences among the reactivities of these precursors, the OHR per C atom in the simulations of all precursors but methane converges near an OH_{exp} of $3x10^{11}$ molecules cm^{-3} s, and then follows a very similar downward trend (Fig. 5b). This OH_{exp} value is roughly where saturated multifunctional species have their maximal relative contribution to the OHR_{VOC} (Figs. 3 and S5). Even in the ambient cases of m-xylene oxidation, saturated multifunctional species also account for about half of OHR_{VOC} when the

https://doi.org/10.5194/acp-2021-118
Preprint. Discussion started: 24 February 2021

Atmospheric Chemistry and Physics Discussions

562 contribution of aromatics, some of which may artificially persist due to mechanism incompleteness, is
563 excluded (Fig. S4). Also, At OH_{exp} > ~$3x10^{11}$ molecules cm^{-3} s, a C atom in saturated multifunctional
564 species on average has at least 0.3 functional groups in the ambient cases (Fig. 4), and the functional
565 group composition is relatively diverse at this OH_{exp}. Therefore, the convergence value of OHR per C
566 atom of ~$2x10^{-12}$ cm^3 $atom^{-1}$ s^{-1} at ~$3x10^{11}$ molecules cm^{-3} s can be largely regarded as a relatively
567 invariant average of those of secondary H and α-H of various O-containing functional groups. Note that
568 this average is for low-NO conditions and can be lower at high NO due to deactivating effects of N-
569 containing groups formed during oxidation (Isaacman-VanWertz and Aumont, 2020).

570 Before the convergence, isoprene has the highest OHR per C atom (on the order of 10^{-11} cm^3 $atom^{-1}$
571 s^{-1}) among the precursors and intermediates/products (Fig. 5b), because of its conjugated C=C bonds.
572 The OHR per C atom of its first-generation oxidation products is slightly lower and close to that of the
573 oxidation intermediates/products of m-xylene, as the main contributors in both cases are oxygenated
574 monoalkenes. The average OHR per C atom of the studied alkanes increases with C number (Fig. 5b),
575 with the upper limit around $1x10^{-12}$ cm^3 $atom^{-1}$ s^{-1} consistent with Kwok and Atkinson (1995), since the
576 less-reactive -CH_3 groups (with OHR per C atom of ~$1x10^{-13}$ cm^3 $atom^{-1}$ s^{-1}) contribute proportionally
577 less to molecular OHR as C number increases. Conversely, the early-stage products of alkane oxidation
578 (mainly alkyl monohydroperoxides) show higher average OHR per C atom for shorter molecules (Fig.
579 5b), owing to the activating (increasing OHR) contribution of the -OOH group.

580 Following the convergence of OHR per C atom, this quantity in all non-methane ambient cases
581 in this study sees a similar decay (Fig. 5b). This coincides with multifunctional species broken into small
582 highly oxidized C1 and C2 compounds. Although among them there are species with OHR per C atom >
583 $5x10^{-12}$ cm^3 $atom^{-1}$ s^{-1} (e.g., CH_3OOH, CH_3CHO, and HCHO), the average OHR per C atom of these C1
584 and C2 species are mainly governed by those reacting more slowly (e.g., HCOOH and particularly CO)
585 and hence reaching higher concentrations amid the fast decay of multifunctional species. The similar fast
586 drop of OHR per C atom after OH_{exp}~$1x10^{12}$ molecules cm^{-3} s for various precursors implies a transition
587 from OHR from saturated multifunctional molecules to OHR from CO before the final oxidation to CO_2
588 (which has zero OHR).

589 **3.6 Total OH consumption for each precursor**

590 Integrating OHR per C atom over OH_{exp} allows us to assess the average number of OH molecules
591 consumed by each C atom during the entire course of oxidation. This quantity can also be apportioned
592 to the contributions of different OH reactants (Fig. 6). Due to incomplete oxidation of several species,
593 especially CO, the value of this quantity for an oxidation with all C atoms ending up with CO_2 should be
594 higher than those at simulation end (OH_{exp}~$4x10^{12}$ molecules cm^{-3} s). We correct this in Fig. 6 by
595 including additional contribution of CO to make its total contribution 1, since CO, the typical penultimate
596 product, consumes one OH molecule in its final oxidation, but is still present in significant quantities at
597 the end of our simulations. Thus, each C atom reacts with OH ~3 times in the course of the oxidation of
598 isoprene and decane to CO_2 (Fig. 6). A simplistic and chemically intuitive explanation for this number
599 is that the average oxidation state ($\overline{OS_C}$) of both isoprene and decane C atoms is ~-2, and needs to increase
600 to the value of +4 in CO_2 at the end of the oxidation. A C1 unit reacting once with OH likely increases
601 its $\overline{OS_C}$ by ~2. This increase is usually realized by an abstraction of H atom by OH or an addition of OH

https://doi.org/10.5194/acp-2021-118
Preprint. Discussion started: 24 February 2021

Atmospheric Chemistry and Physics Discussions

($\overline{OS_C}$ + 1), followed by an abstraction of H atom by O_2 or an addition of O_2 ($\overline{OS_C}$ + 1). Note that ~3 OH consumed per C atom oxidized to CO_2 is likely an upper limit, since the mechanisms in this study do not include RO_2 autoxidation (Crounse et al., 2013; Ehn et al., 2014), which reduces the number of OH needed for complete VOC oxidation. Also, in a real low-NO environment, NO is still present in low concentrations and converts RO_2 to RO. RO may undergo H abstraction through isomerization or reaction with O_2, which also lowers the number of OH needed, although the effect is usually small.

The surprisingly large contribution of hydroperoxy xylenol ($C_8H_{10}O_3$) to OH consumed per C atom in m-xylene oxidation (Fig. 6) is an artifact of mechanism incompleteness. This species may undergo an abstraction of the H atom in its -OOH group by OH. The resulting RO_2 may be converted back to it through a reaction with HO_2. The lack of efficient exit channels from this interconversion artificially sustains it for an extended period, leading to inflated OH consumption.

4 Summary and conclusions

Using the fully explicit GECKO-A model, we simulated OHR evolution in the photooxidation of several types of VOCs (i.e., alkane, alkene, and aromatic) without NO until very high equivalent photochemical ages (>10 d) under a variety of conditions (in the atmosphere, chamber, and OFR). We analyzed the simulations in detail and found a number of common features as well as some differences resulting from certain precursors. They are summarized below:

- All simulated non-methane cases very roughly follow this general oxidation chain pattern: precursor → first-generation products → (second-generation products →) multifunctional species → highly oxidized C1 and C2 species → CO (or HCOOH) → CO_2. These species are generally not at steady state and gain significance/predominance one after another in the entire course of oxidation. Simulation results suggest that fragmentation products are not formed in significant amounts until the late stage of the oxidation, which would be a key difference from studies of OHR evolution in high-NO VOC oxidation (Nakashima et al., 2012; Sato et al., 2017).
- In methane oxidation, the intermediates do not gain dominance in sequence. Instead, they simultaneously increase as the oxidation proceeds, then simultaneously decrease when the methane decay becomes significant. The OHR evolution in methane oxidation is close to the idealized steady-state chain model, as the reaction of methane with OH is orders of magnitude slower than those of its oxidation intermediates, which allows the intermediates to reach their steady state.

The following discussion refers to the non-methane cases.

- Where different types of species dominate OHR_{VOC} in sequence, OHR_{VOC} increases after the current dominant type converts to one with a higher average OHR per C atom, and vice versa. Photooxidations of alkanes and aromatics follow the increasing trend from precursor to saturated multifunctional species (via alkyl monohydroperoxides) and from precursor to unsaturated oxygenated species, respectively. The increase in aromatic oxidation is likely to be more significant, since unsaturated oxygenated species are more reactive than saturated multifunctional species. The conversions from multifunctional species to CO_2 lead to a decay of OHR_{VOC} in both alkane and aromatic photooxidations. OHR_{VOC} in alkene photooxidation is likely to always drop rapidly during C=C bond oxidation and more slowly afterwards.
- C atoms in >C=C<, -CH_2-, and -CH_3 have OHR per C atom on the order of 10^{-11}, 10^{-12}, and 10^{-13} cm^3

https://doi.org/10.5194/acp-2021-118
Preprint. Discussion started: 24 February 2021

Atmospheric Chemistry and Physics Discussions

atom^{-1} s^{-1}, respectively. Together with these values, a relatively weak enhancement of OHR per C atom of a C atom with -OOH substitution can explain the large range spanned by the precursors and their intermediates/products in this study at low OH_{exp}. Around an OH_{exp} of $3x10^{11}$ molecules cm^{-3} s, precursors are largely converted to saturated multifunctional species (e.g., by addition to C=C bonds in unsaturated precursors and abstraction of H atoms in saturated precursors), and the reactive mixtures of those precursors thus have similar OHR per C atom. They then all follow the course: multifunctional species → highly oxidized C1 and C2 species → CO (or HCOOH) → CO_2 and show similar decays of OHR per C atom.

- In decane and isoprene oxidation, our simulations show that each C atom consumes at most ~3 OH molecules in the course of its oxidation to CO_2. This can be simplistically explained as 3 occurrences of oxidation by OH that increase, by 2 each time, the $\overline{OS_C}$ of decane and isoprene (~-2) to that of CO_2 (+4). The total number of OH consumed by each C atom is likely to be lower when RO_2 autoxidation can be included in the mechanism generation.

In general, the OHR evolution differences resulting from different precursors are larger than those due to different conditions. The difference in OHR_{VOC} between the ambient cases with constant and diurnal sunlight is small. Nevertheless, physical conditions may still lead to significant differences, which are summarized below:

- In chambers, gas-wall partitioning can be a prominent issue that causes substantial wall partitioning of certain OVOCs of lower volatility. The clearest example in this study is the near-complete removal of C10 multifunctional species from the gas phase in decane oxidation, and hence the disappearance of the OHR_{VOC} peak. The wall also preferentially absorbs more oxidized (and thus lower-volatility) species, which alters the functional composition of gas-phase multifunctional species. The wall can even serve as a source of multifunctional species at very high OH_{exp}, when the gas-phase concentrations of those species are very low. The magnitude of the effects of wall partitioning also depends on the size of the precursor, with the oxidation of larger precursors in chambers suffering larger impacts of wall partitioning.
- The strong wall losses have important implications, as they can change our modeling results substantially. Systematic OVOC wall partitioning corrections must be made for low-NO oxidation chamber experiments that study OHR_{VOC}. In case of large precursors, highly chemically explicit modeling will likely be necessary to infer the OHR of multifunctional species, which may account for a large fraction of missing reactivity but suffer near-complete wall losses. Although the few existing chamber studies on OHR_{VOC} evolution were all under high-NO conditions, which may result in more fragmentation and higher-volatility products, the magnitude of wall partitioning of large multifunctional species in this study is so substantial that we believe this magnitude would also be important at high NO. Schwantes et al. (2017) considered wall partitioning in their modeling of o-cresol oxidation based on MCM v3.3.1 but still could not achieve good agreement with the measurements for a number of products. Considering this, one should not assume that it is appropriate to neglect wall partitioning in high-NO chamber experiments, just based on agreement between the high-NO chamber experiments and the modeling with MCM-based schemes and without gas-wall partitioning corrections in some literature OHR_{VOC} evolution studies.

https://doi.org/10.5194/acp-2021-118
Preprint. Discussion started: 24 February 2021

Atmospheric Chemistry and Physics Discussions

- OFR has two issues under certain conditions that can cause deviations from the ambient cases in terms of OHR_{VOC}. Strong RO_2 + OH may significantly contribute to OHR_{VOC}. Interestingly, this type of reactions does not seem to be able to substantially alter the composition of OHR_{VOC}. before the OHR_{VOC} peak. Besides, the conditions resulting in strong water vapor photolysis have already been identified as those leading to atmospherically irrelevant RO_2 chemistry in low-NO OFR in previous studies (Peng et al., 2019; Peng and Jimenez, 2020). As long as OFR users follow the guidelines for experimental planning provided in those studies (and use a much lower UV lamp setting), strong RO_2 + OH can be avoided, as shown in Fig. 1.
- The other main issue of OFR is lack of efficient organic photolysis, particularly at high OH_{exp}, when multifunctional species break into highly oxidized C1 and C2 compounds. This problem has been highlighted in previous studies (Peng et al., 2016; Peng and Jimenez, 2020) and been shown again in the present work to be extremely difficult to avoid if a high OH_{exp} is desired. However, the conversion of multifunctional species into highly oxidized C1 and C2 species may not be much slower in OFR than in the atmosphere, since RO_2 + OH, leading to RO formation and subsequently its decomposition, may also play a major role in this conversion. This also results in significantly higher (lower) production of HCHO (CH_3OOH) in OFR than in the atmosphere at high equivalent ages.

With all the key findings in this study presented above, we believe that we have, to some extent, addressed all the three issues for OHR studies raised by Williams and Brune (2015). We largely speciated the likely source of the "missing reactivity", i.e., multifunctional species, by the fully explicit GECKO-A model. A contrast between the technical issues in some isoprene and m-xylene simulations and the high consistency in the other cases highlights the importance of the completeness of the mechanism (even beyond the MCM level) in OHR-related modeling studies. Finally, this study may have opened up the possibility of parameterizing the OHR evolution in (at least low-NO) VOC photooxidation as a function of OH_{exp} only with the often-available knowledge on the first- and second-generation products and the relevant SARs such as Kwok and Atkinson (1995), as the OHR evolution beyond multifunctional species has been shown to be similar for most VOC oxidations. This parametrization may be utilized in regional and global models to better constrain OHR at high equivalent photochemical ages, e.g., in remote regions.

Appendix A: The effect on OH reactivity of non-OH reactions in an OH-driven reaction chain

1) Consider the following reaction chain, where OH is the only oxidant:

$A_1 + OH \rightarrow A_2$, k_1

$A_2 + OH \rightarrow A_3$, k_2

$A_3 + OH \rightarrow A_4$, k_3

…(etc.)

At steady state, $k_1[A_1][OH] = k_2[A_2][OH] = k_3[A_3][OH] = \ldots = C$ (C is a constant).

Then OHR due to individual species, OHR_i, is equal to C/[OH] and is identical for all species.

2) Consider a parallel conversion of A_1 to A_2 by a means other than reaction with OH:

$A_1 + OH \rightarrow A_2$, k_1

$A_1 + B \rightarrow A_2$, k_1', $B \neq OH$

At steady state, $k_1[A_1][OH] + k_1'[A_1][B] = C$.

https://doi.org/10.5194/acp-2021-118
Preprint. Discussion started: 24 February 2021

Atmospheric Chemistry and Physics Discussions

Therefore, $OHR_{A1} = k_1[A_1] < C/[OH]$.

3) Now consider a reaction converting A_1 directly to A_3 occurring in parallel to reaction chain 1),

$A_1 + D \rightarrow A_3$, k_1", $D \neq OH$

$A_1 + OH \rightarrow A_2$, k_1

$A_2 + OH \rightarrow A_3$, k_2

At steady state, $k_1"[A_1][D] + k_2[A_2][OH] = C$

And $OHR_{A1} < C/[OH]$, since $k_1[A_1][OH] = k_2[A_2][OH]$.

Code/Data availability

The chemical mechanisms generated and the outputs of the GECKO-A simulations in this study are available upon request.

Author contribution

ZP and JLJ conceived the study. ZP designed the study. JL-T and ZP performed the simulations. HS, JL-T, ZP, and JLJ developed the GECKO Loader and Plotter. ZP, JL-T, JJO, and BA made updates and developments for GECKO-A. ZP, JL-T, JJO, BA, and JLJ analyzed the results. ZP led the manuscript writing with inputs from all authors.

Competing interests

There are no competing interests to declare.

Acknowledgements

This work was partially supported by NSF AGS-1822664 and AGS-1740610. We thank Sasha Madronich and Alma Hodzic for useful discussions. We would like to acknowledge high-performance computing support from Cheyenne (doi:10.5065/D6RX99HX) provided by NCAR's Computational and Information Systems Laboratory, sponsored by the National Science Foundation.

https://doi.org/10.5194/acp-2021-118
Preprint. Discussion started: 24 February 2021

Atmospheric Chemistry and Physics Discussions

References

Atkinson, R. and Arey, J.: Atmospheric Degradation of Volatile Organic Compounds, Chem. Rev., 103(12), 4605–4638, doi:10.1021/cr0206420, 2003.

Aumont, B., Szopa, S. and Madronich, S.: Modelling the evolution of organic carbon during its gas-phase tropospheric oxidation: development of an explicit model based on a self generating approach, Atmos. Chem. Phys., 5(9), 2497–2517, doi:10.5194/acp-5-2497-2005, 2005.

Ausloos, P. J. and Lias, S. G.: Photochemistry in the Far Ultraviolet, Annu. Rev. Phys. Chem., 22(1), 85–107, doi:10.1146/annurev.pc.22.100171.000505, 1971.

Bloss, C., Wagner, V., Jenkin, M. E., Volkamer, R., Bloss, W. J., Lee, J. D., Heard, D. E., Wirtz, K., Martin-Reviejo, M., Rea, G., Wenger, J. C. and Pilling, M. J.: Development of a detailed chemical mechanism (MCMv3.1) for the atmospheric oxidation of aromatic hydrocarbons, Atmos. Chem. Phys., 5(3), 641–664, doi:10.5194/acp-5-641-2005, 2005.

Brune, W. H.: The Chamber Wall Index for Gas–Wall Interactions in Atmospheric Environmental Enclosures, Environ. Sci. Technol., 53(7), 3645–3652, doi:10.1021/acs.est.8b06260, 2019.

Burkholder, J. B., Sander, S. P., Abbatt, J., Barker, J. R., Huie, R. E., Kolb, C. E., Kurylo, M. J., Orkin, V. L., Wilmouth, D. M. and Wine, P. H.: Chemical Kinetics and Photochemical Data for Use in Atmospheric Studies: Evaluation Number 18, Pasadena, CA, USA. [online] Available from: http://jpldataeval.jpl.nasa.gov/, 2015.

Camredon, M., Aumont, B., Lee-Taylor, J. and Madronich, S.: The SOA/VOC/NO_x system: an explicit model of secondary organic aerosol formation, Atmos. Chem. Phys., 7(21), 5599–5610, doi:10.5194/acp-7-5599-2007, 2007.

Chameides, W., Lindsay, R., Richardson, J. and Kiang, C.: The role of biogenic hydrocarbons in urban photochemical smog: Atlanta as a case study, Science (80-.)., 241(4872), 1473–1475, doi:10.1126/science.3420404, 1988.

Crounse, J. D., Nielsen, L. B., Jørgensen, S., Kjaergaard, H. G. and Wennberg, P. O.: Autoxidation of organic compounds in the atmosphere, J. Phys. Chem. Lett., 4, 3513–3520, doi:10.1021/jz4019207, 2013.

Ehn, M., Thornton, J. a, Kleist, E., Sipilä, M., Junninen, H., Pullinen, I., Springer, M., Rubach, F., Tillmann, R., Lee, B., Lopez-Hilfiker, F., Andres, S., Acir, I.-H., Rissanen, M., Jokinen, T., Schobesberger, S., Kangasluoma, J., Kontkanen, J., Nieminen, T., Kurtén, T., Nielsen, L. B., Jørgensen, S., Kjaergaard, H. G., Canagaratna, M., Maso, M. D., Berndt, T., Petäjä, T., Wahner, A., Kerminen, V.-M., Kulmala, M., Worsnop, D. R., Wildt, J. and Mentel, T. F.: A large source of low-volatility secondary organic aerosol, Nature, 506(7489), 476–479, doi:10.1038/nature13032, 2014.

Cohen, A. J., Brauer, M., Burnett, R., Anderson, H. R., Frostad, J., Estep, K., Balakrishnan, K., Brunekreef, B., Dandona, L., Dandona, R., Feigin, V., Freedman, G., Hubbell, B., Jobling, A., Kan, H., Knibbs, L., Liu, Y., Martin, R., Morawska, L., Pope, C. A., Shin, H., Straif, K., Shaddick, G., Thomas, M., van Dingenen, R., van Donkelaar, A., Vos, T., Murray, C. J. L. and Forouzanfar, M. H.: Estimates and 25-year trends of the global burden of disease attributable to ambient air pollution: an analysis of data from the Global Burden of Diseases Study 2015, Lancet, 389(10082), 1907–1918, doi:10.1016/S0140-6736(17)30505-6, 2017.

Fuchs, H., Novelli, A., Rolletter, M., Hofzumahaus, A., Pfannerstill, E. Y., Kessel, S., Edtbauer, A., Williams, J., Michoud, V., Dusanter, S., Locoge, N., Zannoni, N., Gros, V., Truong, F., Sarda-Esteve, R., Cryer, D. R., Brumby, C. A., Whalley, L. K., Stone, D., Seakins, P. W., Heard, D. E., Schoemaecker, C., Blocquet, M., Coudert, S., Batut, S., Fittschen, C., Thames, A. B., Brune, W. H., Ernest, C., Harder, H., Muller, J. B. A., Elste, T., Kubistin, D., Andres, S., Bohn, B., Hohaus, T., Holland, F., Li, X., Rohrer, F., Kiendler-Scharr, A., Tillmann, R., Wegener, R., Yu, Z., Zou, Q. and Wahner, A.: Comparison of OH reactivity measurements in the atmospheric simulation chamber SAPHIR, Atmos. Meas. Tech., 10(10), 4023–4053, doi:10.5194/amt-10-4023-2017, 2017.

George, I. J. and Abbatt, J. P. D.: Heterogeneous oxidation of atmospheric aerosol particles by gas-phase radicals., Nat. Chem., 2(9), 713–22, doi:10.1038/nchem.806, 2010.

Haagen-Smit, A. J.: Chemistry and Physiology of Los Angeles Smog, Ind. Eng. Chem., 44(6), 1342–1346, doi:10.1021/ie50510a045, 1952.

Hallquist, M., Wenger, J. C., Baltensperger, U., Rudich, Y., Simpson, D., Claeys, M., Dommen, J., Donahue, N. M., George, C., Goldstein, A. H., Hamilton, J. F., Herrmann, H., Hoffmann, T., Iinuma, Y.,

https://doi.org/10.5194/acp-2021-118
Preprint. Discussion started: 24 February 2021

Jang, M., Jenkin, M. E., Jimenez, J. L., Kiendler-Scharr, A., Maenhaut, W., McFiggans, G., Mentel, T. F., Monod, A., Prevot, A. S. H., Seinfeld, J. H., Surratt, J. D., Szmigielski, R. and Wildt, J.: The formation, properties and impact of secondary organic aerosol: current and emerging issues, Atmos. Chem. Phys., 9(14), 5155–5236, 2009.

Hodzic, A., Campuzano-Jost, P., Bian, H., Chin, M., Colarco, P. R., Day, D. A., Froyd, K. D., Heinold, B., Jo, D. S., Katich, J. M., Kodros, J. K., Nault, B. A., Pierce, J. R., Ray, E., Schacht, J., Schill, G. P., Schroder, J. C., Schwarz, J. P., Sueper, D. T., Tegen, I., Tilmes, S., Tsigaridis, K., Yu, P. and Jimenez, J. L.: Characterization of organic aerosol across the global remote troposphere: a comparison of ATom measurements and global chemistry models, Atmos. Chem. Phys., 20(8), 4607–4635, doi:10.5194/acp-20-4607-2020, 2020.

Isaacman-VanWertz, G. and Aumont, B.: Impact of structure on the estimation of atmospherically relevant physicochemical parameters, Atmos. Chem. Phys. Discuss., https://doi.org/10.5194/acp-2020-1038, in review, 2020.

Jenkin, M. E., Saunders, S. M., Wagner, V. and Pilling, M. J.: Protocol for the development of the Master Chemical Mechanism, MCM v3 (Part B): tropospheric degradation of aromatic volatile organic compounds, Atmos. Chem. Phys., 3(1), 181–193, doi:10.5194/acp-3-181-2003, 2003.

Jenkin, M. E., Young, J. C. and Rickard, A. R.: The MCM v3.3.1 degradation scheme for isoprene, Atmos. Chem. Phys., 15(20), 11433–11459, doi:10.5194/acp-15-11433-2015, 2015.

Kang, E., Root, M. J., Toohey, D. W. and Brune, W. H.: Introducing the concept of Potential Aerosol Mass (PAM), Atmos. Chem. Phys., 7(22), 5727–5744, doi:10.5194/acp-7-5727-2007, 2007.

Keller-Rudek, H., Moortgat, G. K., Sander, R. and Sörensen, R.: The MPI-Mainz UV/VIS Spectral Atlas of Gaseous Molecules of Atmospheric Interest, [online] Available from: www.uv-vis-spectral-atlas-mainz.org (Accessed 26 March 2019), 2020.

Kovacs, T. A. and Brune, W. H.: Total OH loss rate measurement, J. Atmos. Chem., 39(2), 105–122, doi:10.1023/A:1010614113786, 2001.

Krechmer, J. E., Pagonis, D., Ziemann, P. J. and Jimenez, J. L.: Quantification of Gas-Wall Partitioning in Teflon Environmental Chambers Using Rapid Bursts of Low-Volatility Oxidized Species Generated in Situ, Environ. Sci. Technol., 50(11), 5757–5765, doi:10.1021/acs.est.6b00606, 2016.

Krechmer, J. E., Day, D. A., Ziemann, P. J. and Jimenez, J. L.: Direct Measurements of Gas/Particle Partitioning and Mass Accommodation Coefficients in Environmental Chambers, Environ. Sci. Technol., 51(20), 11867–11875, doi:10.1021/acs.est.7b02144, 2017.

Kwok, E. and Atkinson, R.: Estimation of hydroxyl radical reaction rate constants for gas-phase organic compounds using a structure-reactivity relationship: An update, Atmos. Environ., 29(14), 1685–1695, doi:10.1016/1352-2310(95)00069-B, 1995.

Levy II, H.: Normal atmosphere: large radical and formaldehyde concentrations predicted., Science, 173(3992), 141–143, doi:10.1126/science.173.3992.141, 1971.

Li, R., Palm, B. B., Ortega, A. M., Hu, W., Peng, Z., Day, D. A., Knote, C., Brune, W. H., de Gouw, J. and Jimenez, J. L.: Modeling the radical chemistry in an Oxidation Flow Reactor (OFR): radical formation and recycling, sensitivities, and OH exposure estimation equation, J. Phys. Chem. A, 119(19), 4418–4432, doi:10.1021/jp509534k, 2015.

Liu, X., Day, D. A., Krechmer, J. E., Brown, W., Peng, Z., Ziemann, P. J. and Jimenez, J. L.: Direct measurements of semi-volatile organic compound dynamics show near-unity mass accommodation coefficients for diverse aerosols, Commun. Chem., 2(1), 98, doi:10.1038/s42004-019-0200-x, 2019.

Lu, K. D., Hofzumahaus, A., Holland, F., Bohn, B., Brauers, T., Fuchs, H., Hu, M., Häseler, R., Kita, K., Kondo, Y., Li, X., Lou, S. R., Oebel, A., Shao, M., Zeng, L. M., Wahner, A., Zhu, T., Zhang, Y. H. and Rohrer, F.: Missing OH source in a suburban environment near Beijing: observed and modelled OH and HO 2 concentrations in summer 2006, Atmos. Chem. Phys., 13(2), 1057–1080, doi:10.5194/acp-13-1057-2013, 2013.

Madronich, S. and Flocke, S.: The Role of Solar Radiation in Atmospheric Chemistry, in Environmental Photochemistry. The Handbook of Environmental Chemistry (Reactions and Processes), vol 2 / 2L, edited by P. Boule, pp. 1–26, Springer, Berlin, Heidelberg., 1999.

Mao, J., Ren, X., Brune, W. H., Olson, J. R., Crawford, J. H., Fried, a., Huey, L. G., Cohen, R. C., Heikes, B., Singh, H. B., Blake, D. R., Sachse, G. W., Diskin, G. S., Hall, S. R. and Shetter, R. E.:

https://doi.org/10.5194/acp-2021-118
Preprint. Discussion started: 24 February 2021

Atmospheric Chemistry and Physics Discussions

856 Airborne measurement of OH reactivity during INTEX-B, Atmos. Chem. Phys., 9(1), 163–173,
857 doi:10.5194/acp-9-163-2009, 2009.

858 Matsunaga, A. and Ziemann, P. J.: Gas-Wall Partitioning of Organic Compounds in a Teflon Film
859 Chamber and Potential Effects on Reaction Product and Aerosol Yield Measurements, Aerosol Sci.
860 Technol., 44(10), 881–892, doi:10.1080/02786826.2010.501044, 2010.

861 Mouchel-Vallon, C., Lee-Taylor, J., Hodzic, A., Artaxo, P., Aumont, B., Camredon, M., Gurarie, D.,
862 Jimenez, J.-L., Lenschow, D. H., Martin, S. T., Nascimento, J., Orlando, J. J., Palm, B. B., Shilling, J.
863 E., Shrivastava, M. and Madronich, S.: Exploration of oxidative chemistry and secondary organic aerosol
864 formation in the Amazon during the wet season: explicit modeling of the Manaus urban plume with
865 GECKO-A, Atmos. Chem. Phys., 20(10), 5995–6014, doi:10.5194/acp-20-5995-2020, 2020.

866 Nakashima, Y., Tsurumaru, H., Imamura, T., Bejan, I., Wenger, J. C. and Kajii, Y.: Total OH reactivity
867 measurements in laboratory studies of the photooxidation of isoprene, Atmos. Environ., 62, 243–247,
868 doi:10.1016/j.atmosenv.2012.08.033, 2012.

869 Nannoolal, Y., Rarey, J. and Ramjugernath, D.: Estimation of pure component properties part 3.
870 Estimation of the vapor pressure of non-electrolyte organic compounds via group contribution and group
871 interactions, Fluid Phase Equilib., 269, 117–133, doi:10.1016/j.fluid.2008.04.020, 2008.

872 Nehr, S., Bohn, B., Fuchs, H., Häseler, R., Hofzumahaus, A., Li, X., Rohrer, F., Tillmann, R. and
873 Wahner, A.: Atmospheric photochemistry of aromatic hydrocarbons: OH budgets during SAPHIR
874 chamber experiments, Atmos. Chem. Phys., 14(13), 6941–6952, doi:10.5194/acp-14-6941-2014, 2014.

875 Nel, A.: Air Pollution-Related Illness: Effects of Particles, Science (80-.)., 308(5723), 804–806,
876 doi:10.1126/science.1108752, 2005.

877 Nölscher, A. C., Butler, T., Auld, J., Veres, P., Muñoz, A., Taraborrelli, D., Vereecken, L., Lelieveld, J.
878 and Williams, J.: Using total OH reactivity to assess isoprene photooxidation via measurement and
879 model, Atmos. Environ., 89, 453–463, doi:10.1016/j.atmosenv.2014.02.024, 2014.

880 Nölscher, A. C., Yañez-Serrano, A. M., Wolff, S., de Araujo, A. C., Lavrič, J. V., Kesselmeier, J. and
881 Williams, J.: Unexpected seasonality in quantity and composition of Amazon rainforest air reactivity,
882 Nat. Commun., 7, 10383, doi:10.1038/ncomms10383, 2016.

883 Orlando, J. J. and Tyndall, G. S.: Laboratory studies of organic peroxy radical chemistry: an overview
884 with emphasis on recent issues of atmospheric significance, Chem. Soc. Rev., 41(19), 6294–6317,
885 doi:10.1039/c2cs35166h, 2012.

886 Pankow, J. F. and Asher, W. E.: SIMPOL.1: A simple group contribution method for predicting vapor
887 pressures and enthalpies of vaporization of multifunctional organic compounds, Atmos. Chem. Phys.,
888 8(10), 2773–2796, doi:10.5194/acp-8-2773-2008, 2008.

889 Peng, Z. and Jimenez, J. L.: Modeling of the chemistry in oxidation flow reactors with high initial NO,
890 Atmos. Chem. Phys., 17(19), 11991–12010, doi:10.5194/acp-17-11991-2017, 2017.

891 Peng, Z. and Jimenez, J. L.: KinSim: A Research-Grade, User-Friendly, Visual Kinetics Simulator for
892 Chemical-Kinetics and Environmental-Chemistry Teaching, J. Chem. Educ., 96(4), 806–811,
893 doi:10.1021/acs.jchemed.9b00033, 2019.

894 Peng, Z. and Jimenez, J. L.: Radical chemistry in oxidation flow reactors for atmospheric chemistry
895 research, Chem. Soc. Rev., doi:10.1039/C9CS00766K, 2020.

896 Peng, Z., Day, D. A., Stark, H., Li, R., Lee-Taylor, J., Palm, B. B., Brune, W. H. and Jimenez, J. L.: HOx
897 radical chemistry in oxidation flow reactors with low-pressure mercury lamps systematically examined
898 by modeling, Atmos. Meas. Tech., 8(11), 4863–4890, doi:10.5194/amt-8-4863-2015, 2015.

899 Peng, Z., Day, D. A., Ortega, A. M., Palm, B. B., Hu, W., Stark, H., Li, R., Tsigaridis, K., Brune, W. H.
900 and Jimenez, J. L.: Non-OH chemistry in oxidation flow reactors for the study of atmospheric chemistry
901 systematically examined by modeling, Atmos. Chem. Phys., 16(7), 4283–4305, doi:10.5194/acp-16-
902 4283-2016, 2016.

903 Peng, Z., Palm, B. B., Day, D. A., Talukdar, R. K., Hu, W., Lambe, A. T., Brune, W. H. and Jimenez, J.
904 L.: Model Evaluation of New Techniques for Maintaining High-NO Conditions in Oxidation Flow
905 Reactors for the Study of OH-Initiated Atmospheric Chemistry, ACS Earth Sp. Chem., 2(2), 72–86,
906 doi:10.1021/acsearthspacechem.7b00070, 2018.

907 Peng, Z., Lee-Taylor, J., Orlando, J. J., Tyndall, G. S. and Jimenez, J. L.: Organic peroxy radical
908 chemistry in oxidation flow reactors and environmental chambers and their atmospheric relevance,

https://doi.org/10.5194/acp-2021-118
Preprint. Discussion started: 24 February 2021

Atmospheric Chemistry and Physics Discussions

909 Atmos. Chem. Phys., 19(2), 813–834, doi:10.5194/acp-19-813-2019, 2019.

910 Sato, K., Nakashima, Y., Morino, Y., Imamura, T., Kurokawa, J. and Kajii, Y.: Total OH reactivity
911 measurements for the OH-initiated oxidation of aromatic hydrocarbons in the presence of NO x, Atmos.
912 Environ., 171, 272–278, doi:10.1016/j.atmosenv.2017.10.036, 2017.

913 Schwantes, R. H., Schilling, K. A., McVay, R. C., Lignell, H., Coggon, M. M., Zhang, X., Wennberg, P.
914 O. and Seinfeld, J. H.: Formation of highly oxygenated low-volatility products from cresol oxidation,
915 Atmos. Chem. Phys., 17(5), 3453–3474, doi:10.5194/acp-17-3453-2017, 2017.

916 Stocker, T. F., Qin, D., Plattner, G.-K., Tignor, M., Allen, S. K., Boschung, J., Nauels, A., Xia, Y., Bex,
917 V. and Midgley, P. M.: Climate Change 2013 - The Physical Science Basis, edited by Intergovernmental
918 Panel on Climate Change, Cambridge University Press, Cambridge., 2014.

919 Stone, D., Whalley, L. K. and Heard, D. E.: Tropospheric OH and HO2 radicals: field measurements and
920 model comparisons, Chem. Soc. Rev., 41(19), 6348, doi:10.1039/c2cs35140d, 2012.

921 Turro, N. J., Ramamurthy, V. and Scaiano, J. C.: Principles of Molecular Photochemistry: An
922 Introduction, University Science Books, Sausalito, CA, USA. [online] Available from:
923 http://www.uscibooks.com/turro2.htm, 2009.

924 Valorso, R., Aumont, B., Camredon, M., Raventos-Duran, T., Mouchel-Vallon, C., Ng, N. L., Seinfeld,
925 J. H., Lee-Taylor, J. and Madronich, S.: Explicit modelling of SOA formation from α-pinene
926 photooxidation: sensitivity to vapour pressure estimation, Atmos. Chem. Phys., 11(14), 6895–6910,
927 doi:10.5194/acp-11-6895-2011, 2011.

928 Verwer, J. G.: Gauss–Seidel Iteration for Stiff ODES from Chemical Kinetics, SIAM J. Sci. Comput.,
929 15(5), 1243–1250, doi:10.1137/0915076, 1994.

930 Verwer, J. G., Blom, J. G., van Loon, M. and Spee, E. J.: A comparison of stiff ODE solvers for
931 atmospheric chemistry problems, Atmos. Environ., 30(1), 49–58, doi:10.1016/1352-2310(95)00283-5,
932 1996.

933 Wennberg, P. O., Bates, K. H., Crounse, J. D., Dodson, L. G., McVay, R. C., Mertens, L. A., Nguyen,
934 T. B., Praske, E., Schwantes, R. H., Smarte, M. D., St Clair, J. M., Teng, A. P., Zhang, X. and Seinfeld,
935 J. H.: Gas-Phase Reactions of Isoprene and Its Major Oxidation Products, Chem. Rev., 118(7), 3337–
936 3390, doi:10.1021/acs.chemrev.7b00439, 2018.

937 Whalley, L. K., Stone, D., Bandy, B., Dunmore, R., Hamilton, J. F., Hopkins, J., Lee, J. D., Lewis, A. C.
938 and Heard, D. E.: Atmospheric OH reactivity in central London: observations, model predictions and
939 estimates of in situ ozone production, Atmos. Chem. Phys., 16(4), 2109–2122, doi:10.5194/acp-16-2109-
940 2016, 2016.

941 Williams, J. and Brune, W.: A roadmap for OH reactivity research, Atmos. Environ., 106, 371–372,
942 doi:10.1016/j.atmosenv.2015.02.017, 2015.

943 Wofsy, S. C., Apel, E., Blake, D. R., Brock, C. A., Brune, W. H., Bui, T. P., Daube, B. C., Dibb, J. E.,
944 Diskin, G. S., Elkiins, J. W., Froyd, K., Hall, S. R., Hanisco, T. F., Huey, L. G., Jimenez, J. L., McKain,
945 K., Montzka, S. A., Ryerson, T. B., Schwarz, J. P., Stephens, B. B., Weinzierl, B. and Wennberg, P.:
946 ATom: Merged Atmospheric Chemistry, Trace Gases, and Aerosols, Oak Ridge, Tennessee, USA., 2021.

947 Yang, Y., Shao, M., Wang, X., Nölscher, A. C., Kessel, S., Guenther, A. and Williams, J.: Towards a
948 quantitative understanding of total OH reactivity: A review, Atmos. Environ., 134(2), 147–161,
949 doi:10.1016/j.atmosenv.2016.03.010, 2016.

950 Zannoni, N., Gros, V., Lanza, M., Sarda, R., Bonsang, B., Kalogridis, C., Preunkert, S., Legrand, M.,
951 Jambert, C., Boissard, C. and Lathiere, J.: OH reactivity and concentrations of biogenic volatile organic
952 compounds in a Mediterranean forest of downy oak trees, Atmos. Chem. Phys., 16(3), 1619–1636,
953 doi:10.5194/acp-16-1619-2016, 2016.

954 Ziemann, P. J. and Atkinson, R.: Kinetics, products, and mechanisms of secondary organic aerosol
955 formation, Chem. Soc. Rev., 41(19), 6582–6605, doi:10.1039/c2cs35122f, 2012.

https://doi.org/10.5194/acp-2021-118
Preprint. Discussion started: 24 February 2021

Atmospheric Chemistry and Physics Discussions

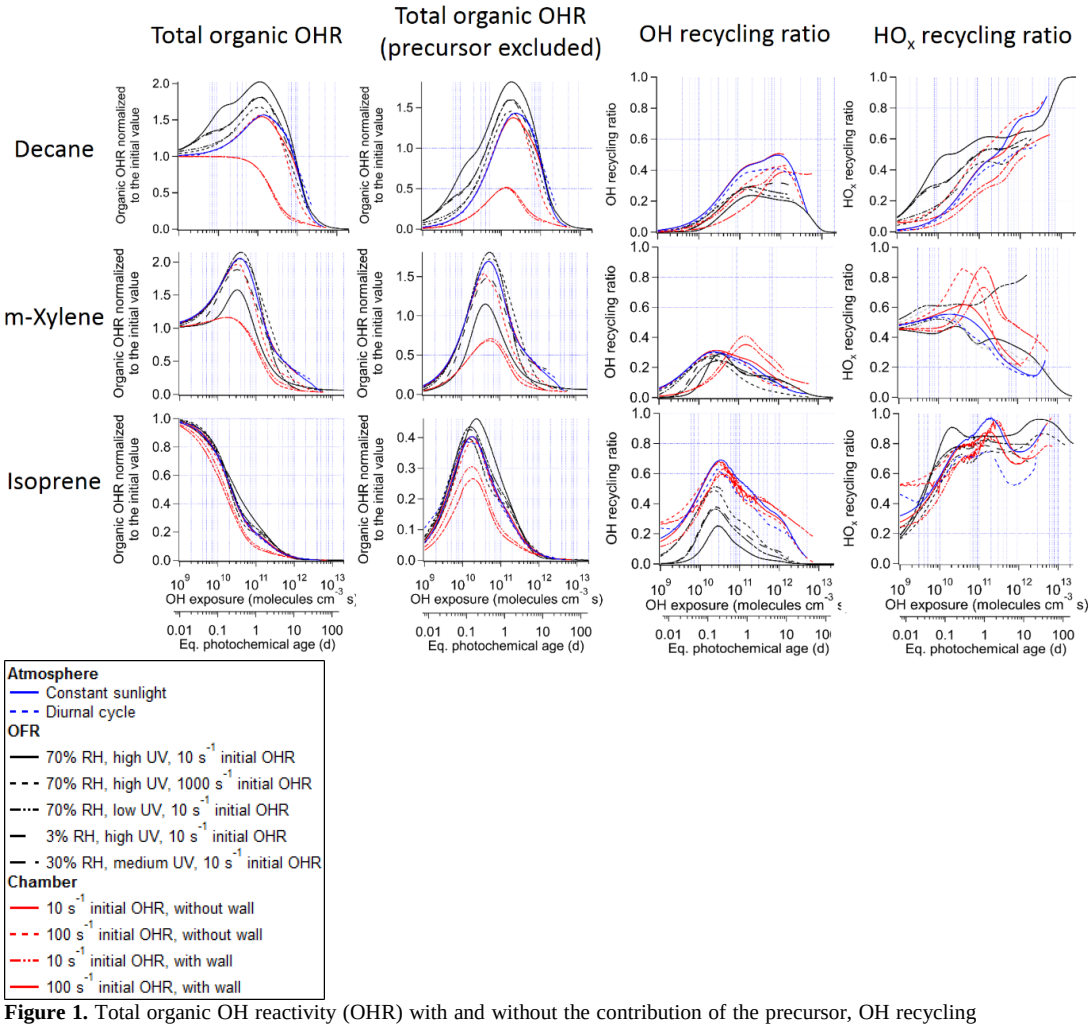

Figure 1. Total organic OH reactivity (OHR) with and without the contribution of the precursor, OH recycling ratio (β_1), and HO_x recycling ratio (β_2) as a function of OH exposure (or equivalent photochemical age; second x-axis) in the photooxidations of decane, isoprene, and m-xylene under different conditions in the atmosphere, oxidation flow reactor (OFR), and chamber.

https://doi.org/10.5194/acp-2021-118
Preprint. Discussion started: 24 February 2021

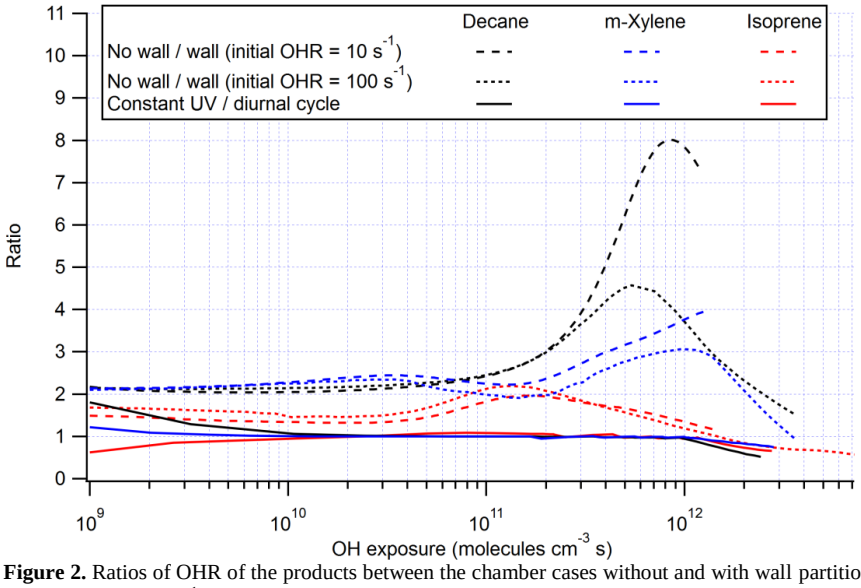

Figure 2. Ratios of OHR of the products between the chamber cases without and with wall partitioning at initial OHR of 10 and 100 s^{-1}, and between the ambient cases with constant and diurnal sunlight for the photooxidations of decane, m-xylene, and isoprene as a function of OH exposure.

https://doi.org/10.5194/acp-2021-118
Preprint. Discussion started: 24 February 2021

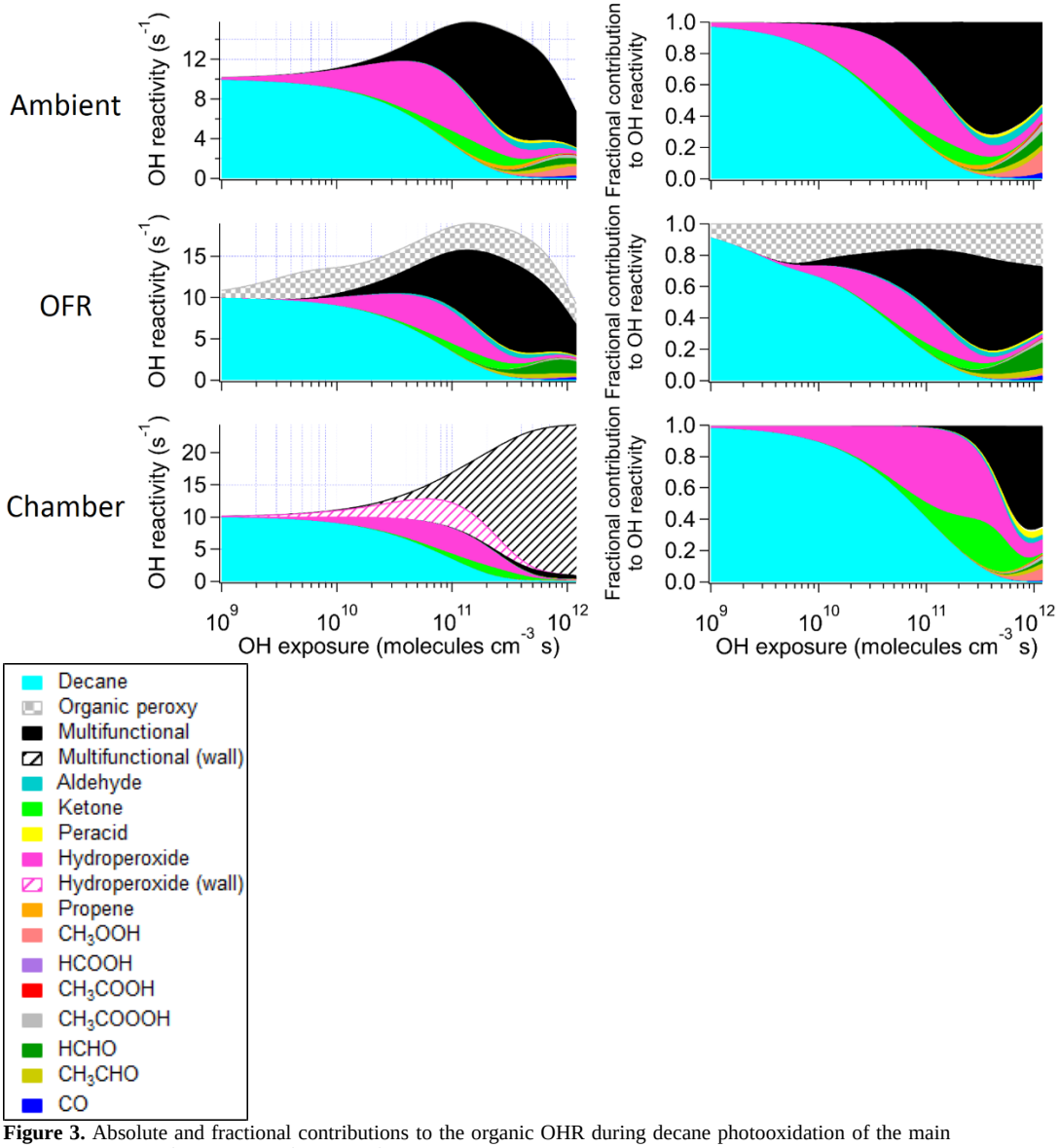

Figure 3. Absolute and fractional contributions to the organic OHR during decane photooxidation of the main species and types of species as a function of OH exposure in the ambient case with constant sunlight; the OFR case with relative humidity of 30%, medium UV lamp setting, and initial OHR of 10 s^{-1}; and the chamber case with initial OHR of 10 s^{-1} and gas-wall partitioning. The types of species shown in this figure exclude the C1 and C2 species listed separately. The OHR of the wall-phase species are the values as if those species are gas-phase OHR contributors, although they actually do not react with OH in the simulations.

https://doi.org/10.5194/acp-2021-118
Preprint. Discussion started: 24 February 2021

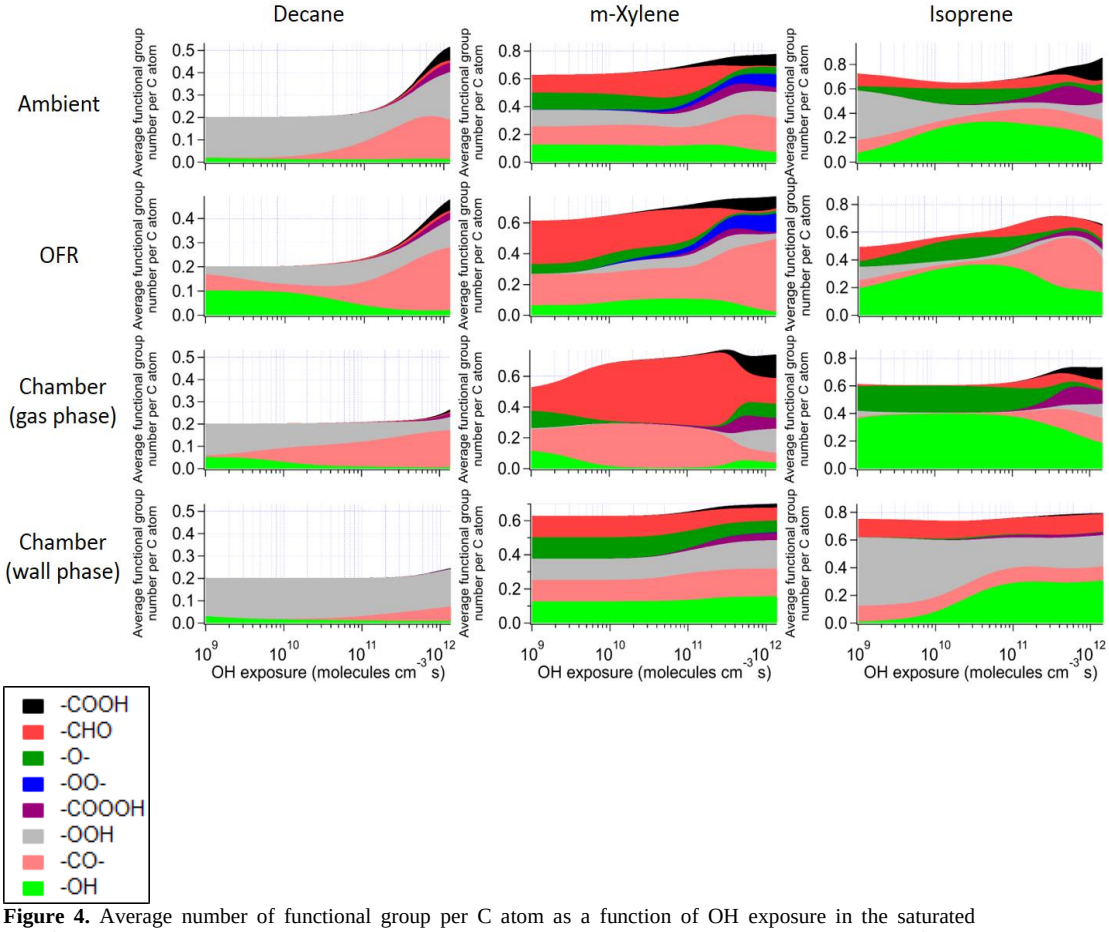

Figure 4. Average number of functional group per C atom as a function of OH exposure in the saturated multifunctional species in the ambient case with constant sunlight, the OFR case with relative humidity of 70%, high UV lamp setting, and initial OHR of 10 s^{-1}, and the gas and wall phases in the chamber case with initial OHR of 10 s^{-1} and gas-wall partitioning of the photooxidations of decane, m-xylene, and isoprene. Note that the functional group "-O-" represents ether, ester, and epoxy groups in the GECKO-A model.

https://doi.org/10.5194/acp-2021-118
Preprint. Discussion started: 24 February 2021

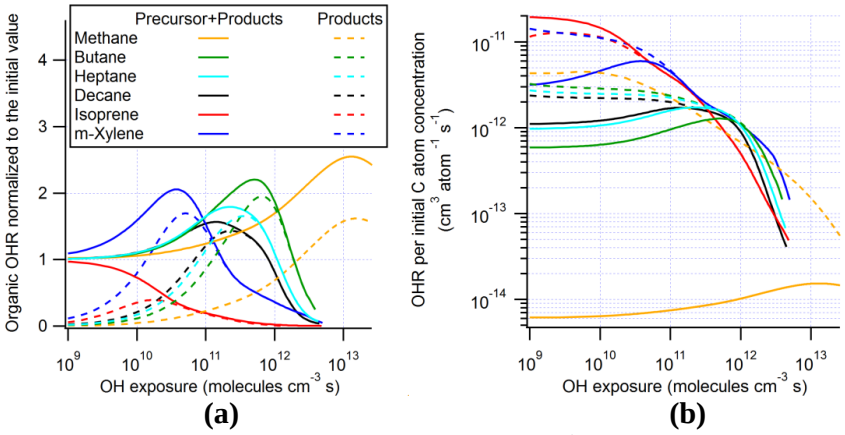

Figure 5. (a) OHR and (b) OHR per initial C atom concentration of the organics (including and excluding the precursor) as a function of OH exposure in the ambient cases with constant sunlight of the photooxidation of methane, butane, heptane, decane, isoprene, and m-xylene.

https://doi.org/10.5194/acp-2021-118
Preprint. Discussion started: 24 February 2021

Atmospheric Chemistry and Physics Discussions

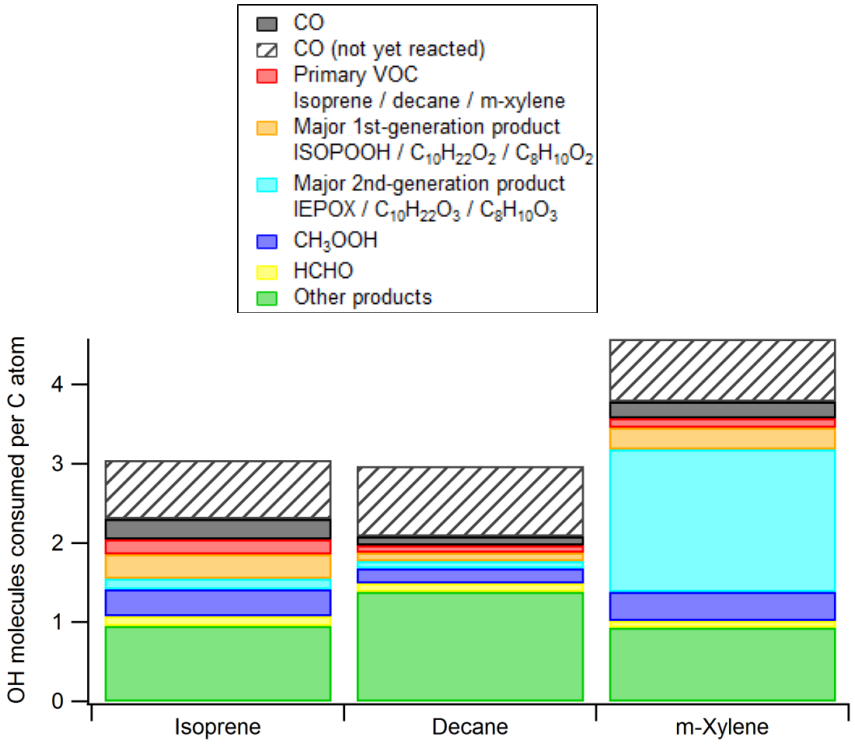

Figure 6. Average numbers of OH molecules consumed per C atom in the ambient cases with constant sunlight during photooxidation of isoprene, decane, and m-xylene. The contribution from CO that is not yet oxidized by OH at the end of simulation is also added to ensure that each CO molecule consumed one OH radical. ISOPOOH, IEPOX, $C_{10}H_{22}O_2$, $C_{10}H_{22}O_3$, $C_8H_{10}O_2$, and $C_8H_{10}O_3$ are isoprene hydroxyl hydroperoxides, isoprene epoxydiols, decyl hydroperoxides, hydroxydecyl hydroperoxides, m-xylenyl hydroperoxide, and hydroperoxy m-xylenol, respectively.

https://doi.org/10.5194/acp-2021-118
Preprint. Discussion started: 24 February 2021

Atmospheric Chemistry and Physics Discussions

Table 1. Conditions and integration timesteps of the simulations in the present work.

Precursor	Environment	Relative humidity (%)	UV	Initial OH reactivity (s^{-1})	Integration timestep (s)
Methane	Ambient	30	Constant sunlight[a]	10	KinSim-determined[b]
	Oxidation flow reactor	70	High lamp setting[c]		
Decane	Ambient	30	Constant sunlight[a]	10	Min: 0.1; Max: 120 (1 d), 300 (2–10 d)
			Diurnal sunlight		
	Oxidation flow reactor	70	High lamp setting[c]	10	0.0025
		70	Low lamp setting[e]	10	
		30	Medium lamp setting[f]	10	
		3	High lamp setting[c]	10	
		70	High lamp setting[c]	1000	
	Chamber (without wall)	30	CU Chamber spectrum[g]	10	Min: 0.1; Max: 120 (6 d), 300 (7–30 d if needed)
				100	
	Chamber (with wall)			10	
				100	
m-Xylene	Ambient	30	Constant sunlight[a]	10	Min: 0.1; Max: 120 (1 d), 300 (2–10 d)
			Diurnal sunlight[c]		
	Oxidation flow reactor	70	High lamp setting[c]	10	0.0025
		70	Low lamp setting[e]	10	
		30	Medium lamp setting[f]	10	
		3	High lamp setting[c]	10	
		70	High lamp setting[c]	1000	
	Chamber (without wall)	30	CU Chamber spectrum[g]	10	Min: 0.1; Max: 120 (6 d), 300 (7–30 d if needed)
				100	
	Chamber (with wall)			10	
				100	
Isoprene	Ambient	30	Constant sunlight[a]	10	Min: 0.1; Max: 10 (1 d), 120 (2–10 d)
			Diurnal sunlight[c]		
	Oxidation flow reactor	70	High lamp setting[c]	10	0.001
		70	Low lamp setting[e]	10	
		30	Medium lamp setting[f]	10	
		3	High lamp setting[c]	10	
		70	High lamp setting[c]	1000	
		30	Medium lamp setting[f] + 5x CU Chamber spectrum[g]	10	
		30	Medium lamp setting[f] + 10000x CU Chamber spectrum[g]	10	
	Chamber (without wall)	30	CU Chamber spectrum[g]	10	Min: 0.1; Max: 10 (6 d), 120 (7–30 d if needed)
				100	
	Chamber (with wall)			10	
				100	
Butane	Ambient	30	Constant sunlight[a]	10	Min: 0.1; Max: 120 (1 d), 300 (2–10 d)
Heptane	Ambient	30	Constant sunlight[a]	10	Min: 0.1; Max: 120 (1 d), 300 (2–10 d)

[a] At solar zenith angle of 45°.
[b] Simulation performed in the solver KinSim, which fully controls its integration timestep selection.
[c] Diurnal variation between solar zenith angles of 0 and 90°.
[d] UV at 185 nm = $1x10^{14}$ photons cm^{-2} s^{-1}; UV at 254 nm = $8.5x10^{15}$ photons cm^{-2} s^{-1}.
[e] UV at 185 nm = $1x10^{11}$ photons cm^{-2} s^{-1}; UV at 254 nm = $4.2x10^{13}$ photons cm^{-2} s^{-1}.
[f] UV at 185 nm = $1x10^{13}$ photons cm^{-2} s^{-1}; UV at 254 nm = $1.4x10^{15}$ photons cm^{-2} s^{-1}.
[g] UV source spectrum of the University of Colorado Environmental Chamber Facility (Krechmer et al.,

https://doi.org/10.5194/acp-2021-118
Preprint. Discussion started: 24 February 2021

Atmospheric Chemistry and Physics Discussions

2017).